ACS Chemical Neuroscience
Cite This: ACS Chem. Neurosci. 2018, 9, 1591−1606
Research Article
pubs.acs.org/chemneuro

A Rational Structured Epitope Defines a Distinct Subclass of Toxic Amyloid-beta Oligomers

Judith M. Silverman,[†,▽] Ebrima Gibbs,[†,▽] Xubiao Peng,[§] Kris M. Martens,[‡] Claudia Balducci,[∥] Jing Wang,[†] Masoud Yousefi,[†] Catherine M. Cowan,[†] Guillaume Lamour,[⊥] Sarah Louadi,[†] Yuxin Ban,[†] Jerome Robert,[‡] Sophie Stukas,[‡] Gianluigi Forloni,[∥] Ging-Yuek R. Hsiung,[#] Steven S. Plotkin,[§] Cheryl L. Wellington,[‡] and Neil R. Cashman*[,†]

[†]Department of Medicine, Djavad Mowafaghian Centre for Brain Health, University of British Columbia, 2211 Wesbrook Mall, Vancouver, BC V6T 2B5, Canada

[‡]Department of Pathology and Laboratory Medicine, Djavad Mowafaghian Centre for Brain Health, University of British Columbia, 2215 Wesbrook Mall, Vancouver, BC V6T 1Z3, Canada

[§]Department of Physics and Astronomy, Genome Sciences and Technology Program, Bioinformatics, Institute for Applied Math, University of British Columbia, Room 311, 6356 Agricultural Road, Vancouver, BC V6T 1Z2, Canada

[∥]IRCCS, Department of Neuroscience, Mario Negri Institute for Pharmacological Research, Via La Masa, 19, 20156 Milano, Italy

[⊥]Chemistry Department, University of British Columbia, Rm D223, 2036 Main Mall, Vancouver, BC V6T 1Z1, Canada

[#]UBC Hospital Clinic for Alzheimer Disease and Related Disorders, Department of Medicine, University of British Columbia, 2215 Wesbrook Mall, Vancouver, BC V6T 1Z3, Canada

Supporting Information

ABSTRACT: Oligomers of amyloid-β (AβO) are deemed key in synaptotoxicity and amyloid seeding of Alzheimer's disease (AD). However, the heterogeneous and dynamic nature of AβO and inadequate markers for AβO subtypes have stymied effective AβO identification and therapeutic targeting *in vivo*. We identified an AβO-subclass epitope defined by differential solvent orientation of the lysine 28 side chain in a constrained loop of serine−asparagine−lysine (cSNK), rarely displayed in molecular dynamics simulations of monomer and fibril ensembles. A mouse monoclonal antibody targeting AβO^{cSNK} recognizes ∼50−60 kDa SDS-resistant soluble Aβ assemblages in AD brain and prolongs the lag phase of Aβ aggregation *in vitro*. Acute peripheral infusion of a murine IgG1 anti-AβO^{cSNK} in two AD mouse models reduced soluble brain Aβ aggregates by 20−30%. Chronic cSNK peptide immunization of APP/PS1 mice engendered an anti-AβO^{cSNK} IgG1 response without epitope spreading to Aβ monomers or fibrils and was accompanied by preservation of global PSD95 expression and improved cued fear memory. Our data indicate that the oligomer subtype AβO^{cSNK} participates in synaptotoxicity and propagation of Aβ aggregation *in vitro* and *in vivo*.

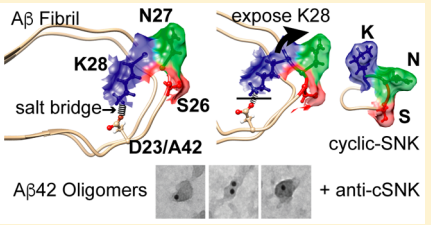

KEYWORDS: *Amyloid-beta oligomers, epitope, Alzheimer's disease, molecular dynamics, neurodegeneration, synaptotoxic*

INTRODUCTION

Polymorphic oligomers of the amyloid β-protein (Aβ) are recognized as the primary toxic Aβ molecular species, responsible directly and indirectly for synaptotoxicity and neurodegeneration in Alzheimer's disease (AD).[1−8] Multiple Phase-III clinical trials of structurally nonselective Aβ immunotherapies have not demonstrated efficacy in primary outcomes, as was reported for bapineuzumab and solanezumab,[9] or caused safety concerns, such as the meningoencephalitis reported in 6% of patients immunized with a fibrillar Aβ vaccine.[10] Therapies targeting Aβ fibrils mobilize soluble Aβ from plaques, which can regenerate toxic AβOs and exacerbate neuronal damage,[11] as well as contribute to amyloid-related imaging abnormalities (ARIA) associated with microhemorrhages and cerebral edema.[12] Thus, we postulate that an ideal therapeutic would specifically target toxic Aβ oligomers and be nonreactive to monomeric Aβ and fibrillar, plaque-associated Aβ.

An assortment of AβO-specific antibodies have been described in the literature[13−20] and shown to improve memory[14,16] or reduce Aβ burden in brain and CSF[21,22] in AD mouse models or both. However, these antibodies were raised or screened against heterogeneous antigens in a discovery-driven approach and are not strictly oligomer specific but cross-react with either monomers or fibrils.[14,17,20,23,24] Similarly, Biogen's fully human aducanumab reacts with Aβ fibrils and oligomers, and while treatment appeared to slow cognitive decline, dose limiting edema, ARIA-E, was induced.[25]

Herein we describe the rational design and validation of a fully AβO-specific epitope, cyclic serine−asparagine−lysine (cSNK).

Received: November 23, 2017
Accepted: April 2, 2018
Published: April 4, 2018

DOI: 10.1021/acschemneuro.7b00469
ACS Chem. Neurosci. 2018, 9, 1591−1606

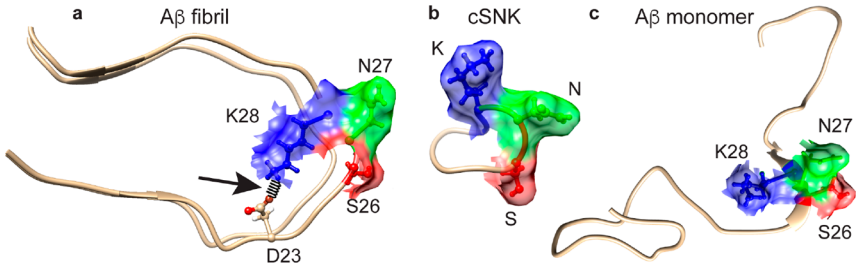

Figure 1. Insoluble Aβ fibrils have a K28−D23 stabilizing salt bridge that may be disrupted in Aβ oligomers. (a) Ribbon diagram of Aβ_{42} fibril structure 2M4J from the Protein Data Bank. Side chains of Lys28 (blue), Asp27 (green), Ser26 (red), and Asp23 (no space filling) are shown. Black spiral between K28 and D23 represents salt bridge. (b) Diagram of the minimal cyclic SNK (cSNK) epitope, with the lysine side chain (blue) oriented into solvent. Side chains of S and N are oriented into solvent in line with the K. (c) Diagram of Aβ_{42} monomer highlighting position of SNK side chains; the K28 side chain is in opposition to those of S26 and N27.

We show that this epitope is specific to a particular toxic and propagative subclass of AβO, designated AβO^{cSNK}. We also show that chronic humoral immune neutralization of AβO^{cSNK} in APP/PS1 mice enables deduction of the pathological roles of this particular AβO subclass *in vivo*, despite the known transience and plasticity of AβOs, a process that could be called "antibody subtraction."

RESULTS AND DISCUSSION

Orientation of Aβ Lysine 28 into Solvent in a Constrained Conformation Engenders a Structure in Agreement with AβO-Specific Qualitative Characteristics. *In vivo,* intrinsically disordered monomeric Aβ peptides undergo conformational changes as AβOs and fibrils form.[26−28] Due to rapid dynamic exchange of conformation and the noncrystalline behavior of AβOs, these structure(s) have not been solved at the atomic level.[29] Structures of Aβ fibrils, which are stable insoluble polymers of Aβ, which have been repeatedly solved, consist of monomers packed into β-hairpin steric zipper structures with residues 18−42 forming a β-turn-β constrained fold/turn stabilized by an internally sequestered salt bridge between the charged residues Lys28 and Asp23 or Glu22[27,30−33] (Figure 1a, black spiral). More recent work has suggested that Lys28 can form a salt bridge with the carboxylic group of Ala42 in Aβ_{42} peptides,[34,35] or Asp1,[36] in contrast to earlier results with Aβ_{40}[32] and Aβ_{42}.[30] In all of these fibril structures, Lys28 participates in a salt bridge that would impair antibody recognition, likely requiring the free epsilon amino group of Lys28. In contrast, AβOs are soluble,[37] and though the structure is unknown and thought to be highly dynamic, low-resolution characterization of AβOs using atomic force microscopy, electron microscopy, and other methods suggest that quasi-stable local structures can exist.[27,38]

We hypothesized that solvent exposure of the Lys28 side chain, in contrast to sequestration of the Lys28 side chain in a salt bridge within Aβ_{40} and Aβ_{42} fibrils,[30,32,34,35] would be in keeping with the known solubility and instability of AβO compared to fibrils. We proposed that the solvent-exposed Lys, in the structurally constrained context of the β-turn, serine−asparagine−lysine (SNK), might constitute an epitope unique to soluble AβOs (Figure 1b). In contrast, monomeric Aβ would adopt myriad SNK motif conformations and side chain orientations (Figure 1c), unlikely to adopt the simultaneous constrained turn and side chain exposure of SNK, unless perhaps at the genesis of oligomer formation.

The cSNK AβO epitope contrasts with some previous molecular models of AβO, which include the internal K28−D23 salt-bridge explicitly demonstrated in fibrils.[27,30] In contrast to these inferred structures, high resolution nuclear magnetic resonance spectroscopy (NMR) of AβO$_{40}$ has demonstrated a contact between K28 and G29, indicating a disruption of the internal salt bridge with D23.[39] Moreover, investigations of AβO$_{42}$ found amide exchange rates that suggested a solvent-accessible turn at Gly25−Gly29,[27] consistent with our hypothesis. We speculate that both lysine orientation structures, solvent sequestered[27,30,39] and exposed, may coexist in the dynamic populations of AβO. Moreover, it may be that the lysine exposed structures are the predominately toxic species,[40,41] as indicated by the role for lysine in Aβ membrane pore formation.[42]

To mimic the constrained β-turn structure of Aβ fibrils and the solvent exposed Lys28 orientation of the hypothesized AβO-specific epitope cSNK, a peptide containing the native Aβ sequence GSNKG was synthesized. The peptide was cyclized by two methods: flanked with non-native cysteines and cyclized via disulfide oxidation, Cys−Cys (Supporting Figure 1a), or synthesized as CGSNKGG and cyclized head-to-tail through a peptide bond, Cys−Gly (Supporting Figure 1c). We used the disulfide oxidation cyclization when initially generating monoclonal antibodies, which could be effectively screened and selected from antibodies reactive with reduced linearized peptide. However, for vaccine immunization in which antibody selection could not be performed, we chose a more stable cyclic peptide structure (head-to-tail) that could not be reduced to linear forms. Unstructured linear peptides of the same sequences were synthesized for control purposes (Supporting Figure 1b,d).

Molecular Dynamics Simulations Confirm Minimal Structural Overlap of cSNK, Monomer, and Fibrillar Aβ Structural Ensembles. We tested the hypothesis that the structured cSNK epitope differs from the structures of Aβ monomers and fibrils using molecular dynamics (MD) simulations. For simulation details, see Materials and Methods. Briefly, an initial configuration of the cSNK epitope was constructed *in silico*, while an Aβ_{40} fibril structure was taken from Protein Data Bank 2M4J.[43] Extended MD equilibration simulation from each initial configuration produced thousands of possible structures, together constituting the equilibrium ensembles for cSNK and the Aβ fibril used in subsequent analysis. For the intrinsically disordered Aβ monomer, we constructed multiple initial configurations from Protein Data Bank 1Z0Q structure. MD equilibrations for each initial monomer configuration were collected and pooled to generate the monomer equilibrium ensemble.

Definitive evidence that the sequence GSNKG displays a different conformation in the context of the cyclic peptide than in either monomeric Aβ_{42} or the fibril can be seen by plotting a fictional, nonbonded dihedral angle that determines the relative

DOI: 10.1021/acschemneuro.7b00469
ACS Chem. Neurosci. 2018, 9, 1591−1606

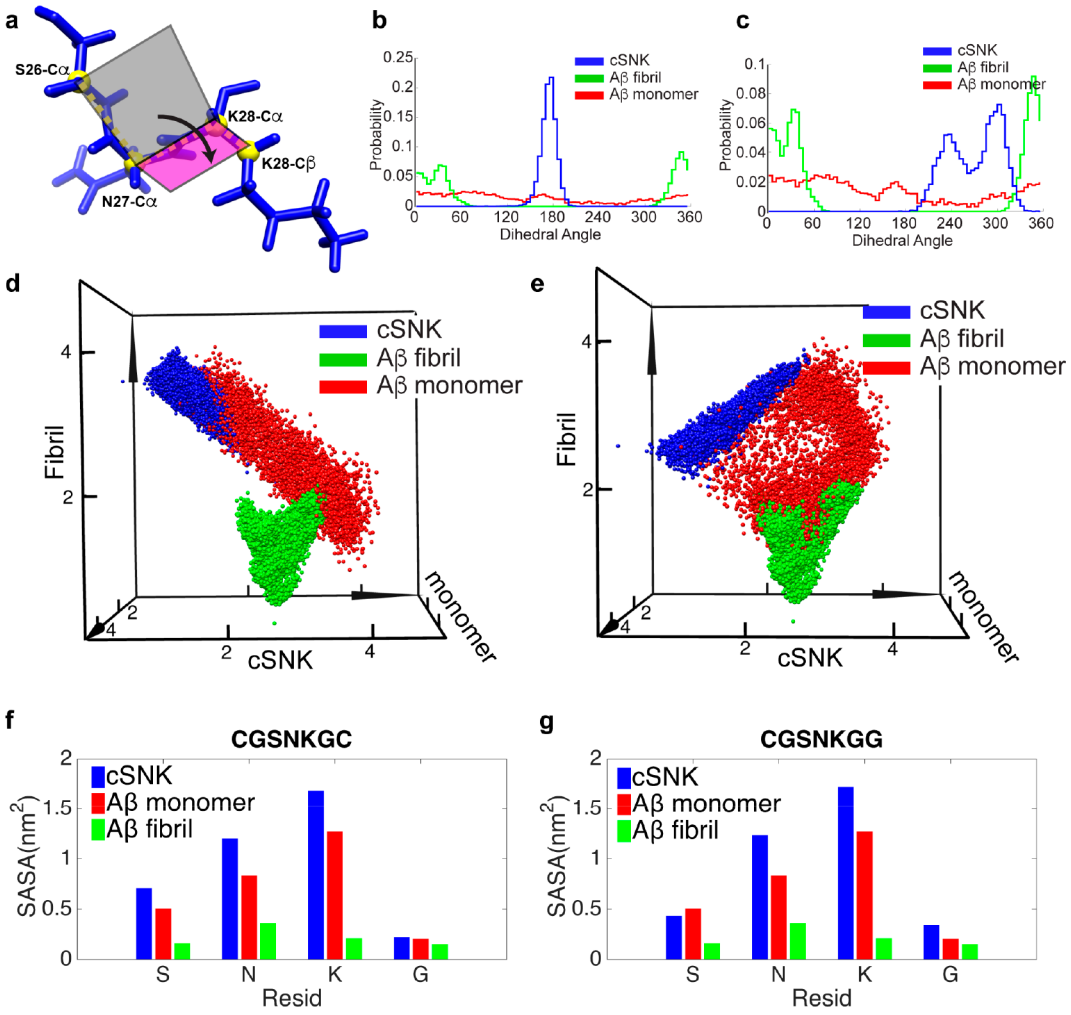

Figure 2. The cSNK epitope is structurally distinct from fibrillar and monomeric Aβ. (a) Diagram of the fictional dihedral angle (arrow) formed between the plane defined by the S26, N27, and K28 Cα atoms (gray plane) and the plane defined by the N27, K28 Cα, and K28 Cβ (pink plane) for the c[CGSNKGC] peptide. (b, c) Dihedral angle probability distributions. The probability of each conformation to take on a certain dihedral angle is shown in panel b for c[CGSNKGC] and in panel c for c[CGSNKGG]. (d, e) Axes correspond to the root mean squared deviation (RMSD) values from the centroids of the Aβ monomer ensemble (red), fibril ensemble (green), and cyclic peptide ensemble (blue) for the peptides c[CGSNKGC] (d) and c[CGSNKGG] (e). Each point corresponds to a given conformation taken from either the cyclic peptide (blue), fibril structure (green), or Aβ monomer (red) equilibrium ensembles. The structural ensembles of the cyclic, monomeric, and fibril species are significantly different. (f, g) Side chain solvent-accessible surface area (SASA) of residues S26−G29, for the cSNK, monomeric Aβ_{42}, and Aβ_{40} fibril equilibrium ensembles (PDB 2M4J[43]) in c[CGSNKGC] (f) and c[CGSNKGG] (g). The cyclic species shows more solvent exposure than either the monomer or fibril, particularly for residue K28.

orientation of the Lys28 side chain with respect to Ser26 and Asn27—the dihedral angle between the Ser26, Asn27, and Lys28 Cα atoms and the Asn27 Cα, Lys28 Cα, and Lys28 Cβ atoms (Figure 2a). For each equilibrium ensemble (cSNK, Aβ monomer, Aβ fibril), this angle was calculated for all configurations and the corresponding distribution was determined. As shown in Figure 2b, cyclized CGSNKGC (c[CGSNKGC]) has a substantial probability peak (0.2) at dihedral angle 180°, whereas no such peak is found for Aβ_{42} monomers or the Aβ_{40} fibril ensemble (PDB 2M4J); the fibril ensemble has two small peaks (0.05−0.075) around dihedral angles 300° and 60°. The sharply peaked dihedral angle for the cSNK ensemble indicates a more constrained conformation. A similar pattern is seen for c[CGSNKGG], though for this peptide two predominant probability peaks (0.05−0.07) for cSNK are seen at slightly higher dihedral angles of 240° and 300° (Figure 2c). For both c[CGSNKGC] and c[CGSNKGG], the cSNK dihedral angle is clearly different from those of either monomers or fibrils, unambiguously demonstrating that cSNK maintains a distinct structure.

Further evidence of a distinct structural ensemble for the cyclic peptide can be seen using structural alignment metrics between the Aβ monomer, fibril, and cSNK equilibrium conformational ensembles, and then implementing clustering analysis. Using clustering analysis of the root mean squared deviation (RMSD) between conformations within an ensemble, the centroid GSNKG structure of the largest cluster in the equilibrium ensembles in the context of cSNK, monomeric Aβ, and the Aβ fibril may be found. The centroid is the structure with the smallest distance in RMSD from all other MD generated structures for each ensemble interrogated, namely, cSNK, Aβ monomer, and fibril.

For each configuration in any ensemble, the three RMSD values between that configuration and the three centroids mentioned above may be calculated and plotted as a point in 3D. As a result, all the configurations can be visualized in a 3D scatter plot, to determine whether the cSNK, Aβ monomer, and fibril ensembles are distinct. It is evident from Figure 2d,e that the cSNK, monomeric, and fibril ensembles cluster differently from each other. We observed no overlap between the fibril and cyclic

DOI: 10.1021/acschemneuro.7b00469
ACS Chem. Neurosci. 2018, 9, 1591−1606

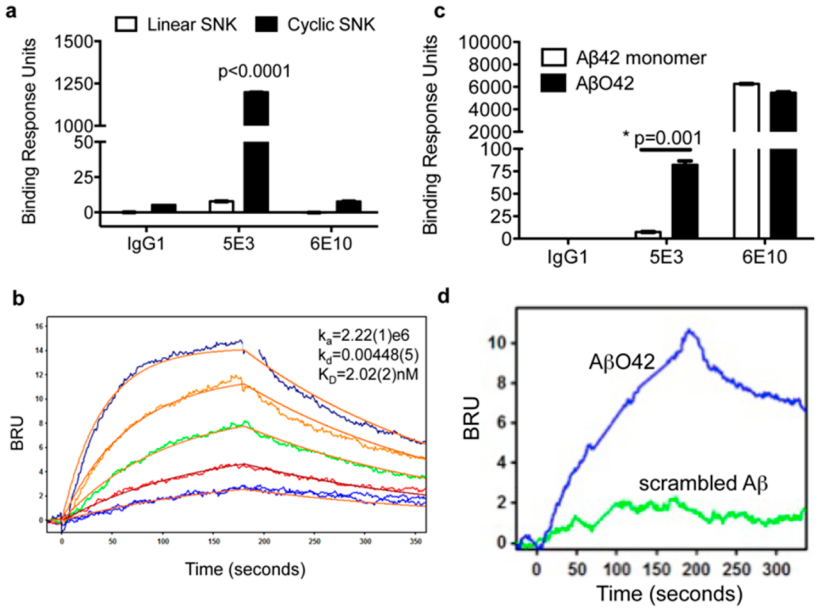

Figure 3. The cSNK epitope is specific to cyclic peptide and Aβ oligomers. (a) SPR measurements of mAb anti-AβO^{cSNK} binding to cognate peptide epitope (cyclic-SNK) and linear SNK peptide. Mean and SEM from three identical experiments are shown. Differences were determined by two-way ANOVA with Bonferonni's multiple comparisons test, anti-AβO^{cSNK}−cyclic-SNK is different from all other samples ($p < 0.0001$). (b) Representative sensorgrams of 2-fold serial dilutions of anti-AβO^{cSNK} (from 4.7 nM to 75 nM) binding to immobilized cSNK. Three identical experiments were performed. (c) SPR measurements of antibody binding to Aβ_{42} monomers and Aβ_{42} oligomers (AβO$_{42}$). Means and SEM of six identical experiments are shown. Differences were determined by two-way ANOVA with Bonferonni's multiple comparison test. (d) Representative SPR sensogram measuring anti-AβO^{cSNK} binding to Aβ_{42} oligomers and scrambled Aβ_{42} peptide prepared under oligomer-forming conditions immobilized to the sensor chip. Sensorgrams were double-referenced by subtracting binding responses on the reference surface and buffer blanks.

ensembles (Figure 2d,e). As well, only 4% and 8% of monomeric ensembles appear in the corresponding ensemble regions for peptides c[CGSNKGC] and c[CGSNKGG], respectively (Figure 2d,e and Supporting Figure 1e,f). The cSNK structural ensemble is thus distinct from either the Aβ monomeric or fibril ensembles, indicating that antibodies specific to the cSNK will likely have low affinity to the conformations presented in the monomer or fibril ensembles.

In addition to this distinct conformation, we hypothesized that the cSNK would uniquely expose the lysine side chain to solvent. The solvent-accessible surface area (SASA)[44,45] of the amino acid side chains, as probed by a particle of water radius 1.4 Å, was determined for residues GSNKG in the context of cSNK, monomeric Aβ_{42}, and fibrils. The results for the two peptides c[CGSNKGC] and c[CGSNKGG] were nearly identical in these experiments (Figure 2f,g). Lysine in the cyclic peptide shows the most solvent exposure, significantly more than that in monomeric Aβ_{42} or fibril. This is in agreement with our hypothesis that the biggest increase in exposure between cSNK and fibrils is observed for residue Lys28 (Figure 2f,g). Together, the dihedral angle, RMSD plots, and SASA *in silico* analyses confirm the unique structure and lysine solvation of the cSNK epitope.

The GSNKG motif corresponding to the native Aβ sequence containing the cSNK epitope was screened against the PDB to determine whether this motif appears in human proteins of known structure. The motif GSNKG was found in 46 human protein entries, 43 of which are associated with the Aβ peptide or APP protein itself. The remaining three PDB entries, 1ZGL, 4P4K, and 4QRP, all correspond to the α chain of the variable domain of T-cell receptor protein, in which the potential cross-reactive sequence is buried in a solvent- and antibody-inaccessible form (Supporting Figure 1h, inset panels, GSNKG motif in orange). To determine if the motif takes the constrained and side chain exposed conformation of the cSNK epitope, we subjected the T cell receptor α GSNKG regions to SASA analysis. The SASA for the cryptic motif in the "off-target" PDB structures ranged from 100 to 160 Å^2, substantially lower than the surface area exposed by the cSNK epitope, 350−450 Å^2 (Supporting Figure 1h), implying minimal target distraction by cSNK cognate antibodies due to the off-target protein.

Mice Immunized with cSNK Peptides Generate Antibodies Specific to AβOs. To test our hypothesis that cSNK is an AβO-specific epitope, we generated anti-cSNK monoclonal antibodies in mice immunized with disulfide-cyclized cSNK-PEG2 conjugated to KLH. Screening of hybridoma IgGs identified a cSNK-specific lead clone, an IgG1 designated anti-AβO^{cSNK}, which bound to cSNK peptide but not to the SNK linear peptide (Figure 3a). Neither peptide was recognized by an IgG1 isotype control or by the pan anti-Aβ 6E10 antibody (Figure 3a), the cognate epitope of which spans amino acids 1−6 from the N-terminus of the Aβ peptide. A detailed affinity analysis found that the lead clone bound to BSA-conjugated cSNK with a mean dissociation constant (K_D) of 2.02 nM (Figure 3b).

Anti-AβO^{cSNK} bound specifically to synthetic Aβ_{42} oligomers (AβO$_{42}$) and showed negligible binding to monomeric Aβ_{42} (p = 0.001, Figure 3c). The constrained turn configuration of cSNK likely accounts for the lack of cross-reactivity to ∼95% of Aβ monomer conformations (Figure 3c), which are intrinsically disordered, and for which the GSNKG motif is highly dynamic, with minimal conformational overlap with constrained cyclic-SNK (Figure 2).[27] In contrast, 6E10 did not differentiate between monomers and AβOs (Figure 3c).

In our characterization of the synthetic Aβ monomers, AβO$_{42}$, and fibrils that we generated to test the oligomer specificity of the cSNK epitope (Figures 3−5), we and others have observed that

DOI: 10.1021/acschemneuro.7b00469
ACS Chem. Neurosci. 2018, 9, 1591−1606

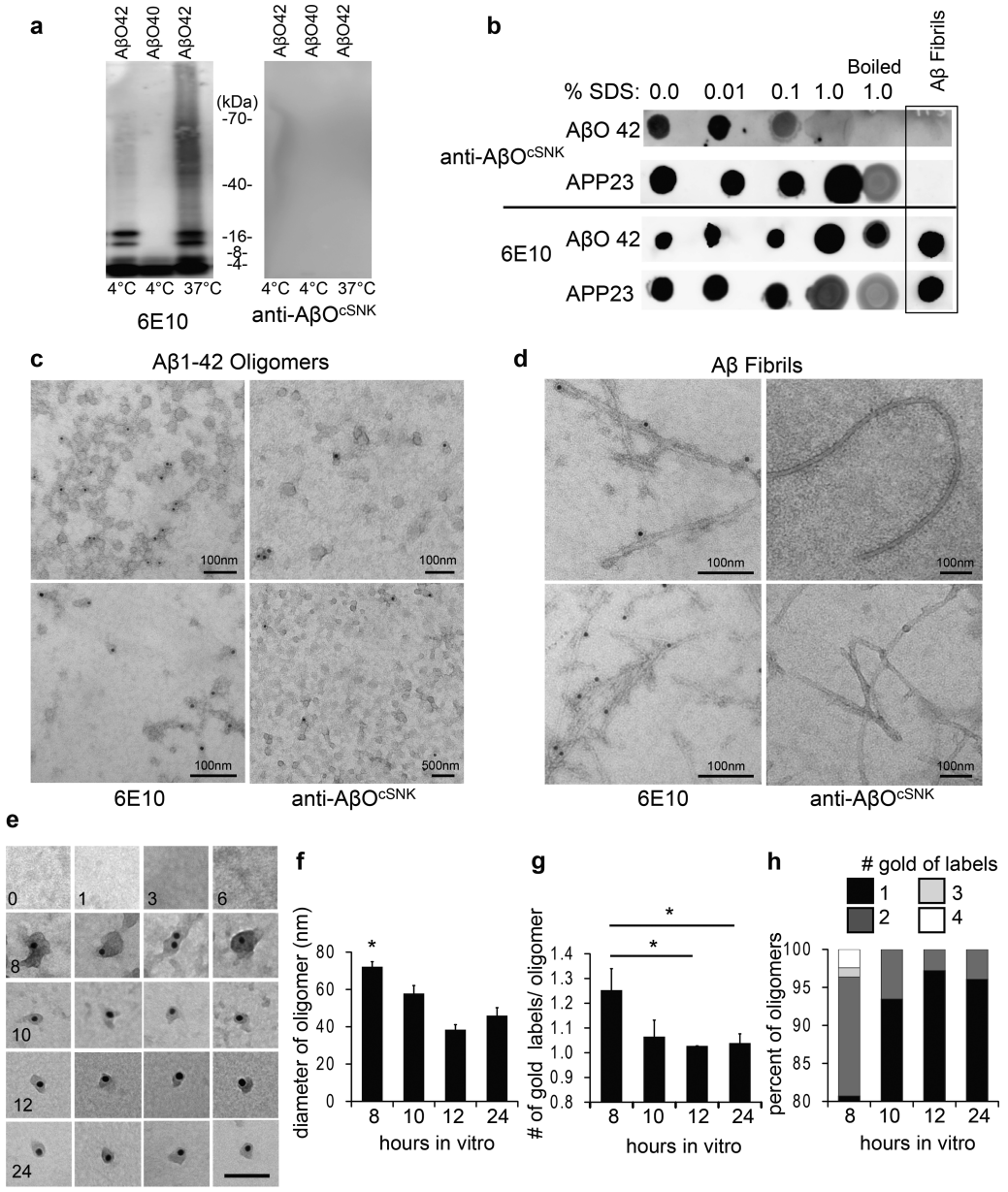

Figure 4. cSNK epitopes are found in brain-derived and synthetic AβO populations, are absent from Aβ fibrils, and are maximally displayed by newly formed synthetic $AβO_{42}$. (a) Aβ oligomers generated at different temperatures from either $Aβ_{42}$ peptide ($AβO_{42}$) or $Aβ_{40}$ peptide ($AβO_{40}$) fractionated by SDS-PAGE and immunoblotted with 6E10 or anti-$AβO^{cSNK}$. Data is representative of at least four identical experiments. (b) $AβO_{42}$ (5 μg) and APP23 (1 μg) soluble brain extract incubated with increasing amounts of SDS for 1 h at 37 °C or boiled for 10 min with 1% SDS prior to dot blotting. Five micrograms of $Aβ_{42}$ fibrils was also dotted onto the membrane (box). When probing membranes with high affinity 6E10, only 0.5 μg of $AβO_{42}$ was dotted. Membranes were probed with anti-$AβO^{cSNK}$ (150 μg/mL) and 6E10 (1 μg/mL). Data is representative of four experiments. (c,d) Immunoelectron micrographs of $Aβ_{42}$ oligomers (c) and fibrils (d), probed with either anti-$AβO^{cSNK}$ or 6E10. Replicate grids were imaged; data are representative of two identical experiments. (e) Representative electron micrographs of individual $Aβ_{42}$ oligomers labeled with anti-$AβO^{cSNK}$ sampled and imaged at 8, 10, 12, and 24 h, post-resuspension of monomer film. Scale bar = 100 nm. (f–h) Unbiased sampling of 35–60 fields of view per time point at 60 000× magnification yielded 45–80 labeled oligomers per time point. Data is from one of two representative experiments; SEM is shown. (f) The mean diameter of anti-$AβO^{cSNK}$-labeled $AβO_{42}$ for each time point shows that the oligomers decrease in diameter over time. Unlabeled $AβO_{42}$ were excluded from analysis. One-way ANOVA with Bonferroni correction reports statistical differences between 8 and 10 h ($p = 0.05$), between 8 and 12 h ($p = 0.001$), and between 8 and 24 h ($p = 0.001$). (g) The mean number of anti-$AβO^{cSNK}$ grains per $AβO_{42}$ for each time point shows that the number of anti-$AβO^{cSNK}$ bound to $AβO_{42}$ decreases as the diameter decreases. Unlabeled $AβO_{42}$ were excluded from analysis. One-way ANOVA with Bonferroni correction reports statistical differences between 8 and 12 h and between 8 and 24 h. (h) This data are represented as percentage of oligomers with each number of antibody labels.

the aggregation-prone nature of $Aβ_{42}$ obviates the maintenance of a pure Aβ monomer solution, as aggregation begins immediately once the peptides are resuspended in solution;[39] this may explain the minor anti-$AβO^{cSNK}$ reactivity to our monomeric solution (Figure 3c).

We characterized synthetic $Aβ_{42}$ preparations by atomic force microscopy (Supporting Figure 2a). The height distribution of Aβ monomer preparations centers around 0.4 nm; however, apparently spherical objects up to 1 nm height are detected. The height distribution of $AβO_{42}$ ranged from 0.3 to ~4.0 nm, with a

DOI: 10.1021/acschemneuro.7b00469
ACS Chem. Neurosci. 2018, 9, 1591–1606

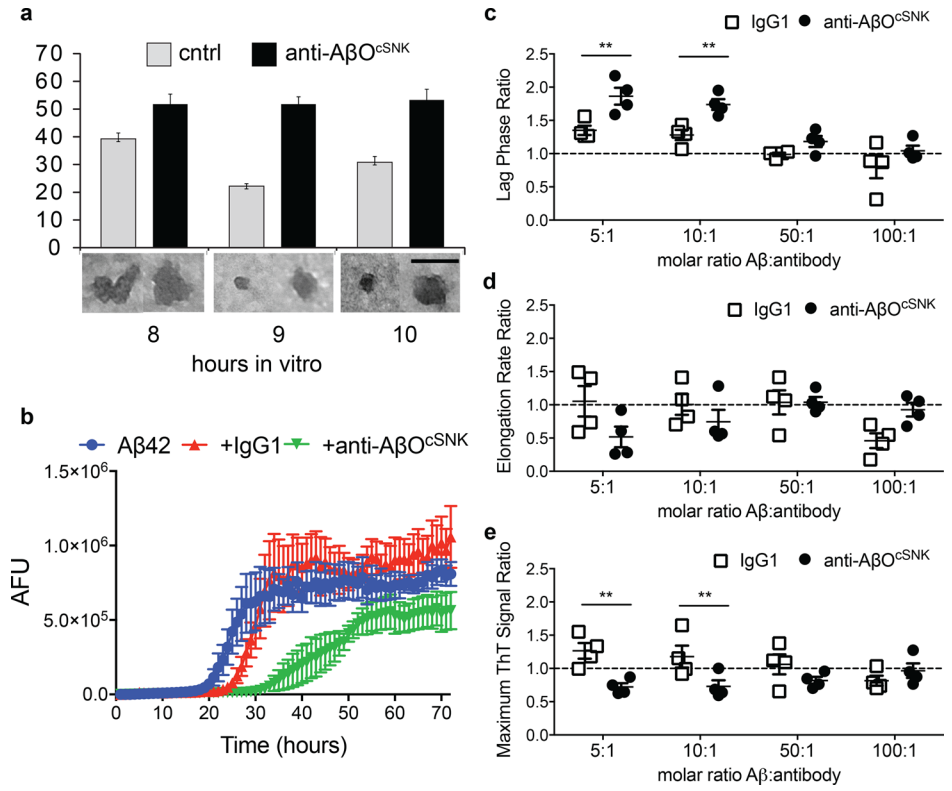

Figure 5. Anti-AβO^{cSNK} binding delays synthetic AβO$_{42}$ maturation. (a) The mean diameter of AβO$_{42}$ at 8, 9, and 10 h of monomer incubation with anti-AβO^{cSNK} (black) or without antibody (gray). Two-way ANOVA reports a treatment effect of 0.0029. Data represent one of two experiments. Unbiased sampling of 8 fields of view per time point at 60 000× magnification yielded 25−110 oligomers per time point per experiment; SEM is shown. Below, representative electron micrographs of individual AβO$_{42}$ with and without anti-AβO^{cSNK} co-incubation sampled at different times. Scale bar = 100 nm. (b) β-Sheet formation was tracked for 72 h *in vitro* by a thioflavin T fluorescent assay after addition of Aβ monomers alone or in the presence of either anti-AβO^{cSNK} or a nonspecific IgG1 isotope control at a molar ratio of 5:1 Aβ/antibody. Data presented are the means from four identical experiments with SEM. (c−e) Data are presented as a ratio with SEM of the Aβ_{42} plus anti-AβO^{cSNK} or IgG1 signal over the Aβ_{42} signal alone to compare the effectiveness of anti-AβO^{cSNK} in impeding Aβ aggregation. Differences were determined by two-way ANOVA with Bonferonni's multiple comparison tests. (c) At 5:1 and 10:1 Aβ/antibody molar ratios, anti-AβO^{cSNK} significantly lengthens the lag phase compared to IgG1 control (** $p < 0.01$). (d) The elongation rate is not significantly impacted in the presence of anti-AβO^{cSNK} compared to IgG1. (e) anti-AβO^{cSNK} diminishes the final β-sheet content as measured by ThioT fluorescence, compared to Aβ alone and with IgG1 control, significantly at 5:1 and 10:1 Aβ/antibody molar ratios (**$p < 0.01$). Two-way ANOVA shows a significant difference between anti-AβO^{cSNK} and IgG1 in their effect on the lag phase ($p < 0.0001$) and the maximum β-sheet levels ($p = 0.003$).

mean value of 1.5 nm. The corresponding height of the largest objects in the monomeric solution with the mean height of the AβO solution is consistent with the monomers being contaminated with occasional AβOs. Similarly, fibrils display a range of heights, which overlap with the oligomer range (Supporting Figure 2a), demonstrating, as others have, that fibril preparations are highly heterogeneous and include monomers, oligomers, and fibrils.[39,46] The heterogeneity of Aβ fibril preparations would assert implicit ambiguity upon an SPR binding experiment, and more specific localization methods are required, such as immuno-electron microscopy (Figure 4).

To confirm that the GSNKG sequence itself is required for anti-AβO^{cSNK} recognition, we compared anti-AβO^{cSNK} binding to AβOs and to scrambled Aβ_{42} peptides lacking the GSNKG motif that were prepared following our oligomer-forming protocol. Anti-AβO^{cSNK} had essentially no binding to scrambled peptides, while AβOs were bound robustly by anti-AβO^{cSNK} (Figure 3d).

Heterogeneous synthetic AβO$_{42}$ generated via published protocols[37,47] were detected by 6E10 immunoblotting after SDS-PAGE (Figure 4a), indicating that some AβO$_{42}$ may be SDS-resistant. Alternatively these bands may represent SDS-induced assembly of lower-order species.[48] However, anti-AβO^{cSNK} did not reproducibly recognize any authentic bands under these conditions (Figure 4a), suggesting that the subset of synthetic AβO displaying the cSNK epitope are SDS sensitive. In a dot blot assay, untreated synthetic AβO$_{42}$ were recognized by anti-AβO^{cSNK}, while AβO$_{42}$ incubated in 1% SDS or boiled in SDS showed no reactivity to anti-AβO^{cSNK} (Figure 4b), confirming the SDS sensitivity of synthetic AβO^{cSNK}. In contrast, 6E10 recognized all forms of Aβ_{42}, as expected for an unstructured epitope. As expected, blotted Aβ fibrils were recognized by 6E10 but were not detected by anti-AβO^{cSNK} (Figure 4b).

Interestingly, the pattern of immunoreactivity for AβOs from AD mouse model APP23 soluble brain extracts (and human AD brain AβO; *vide infra*) was different than that of synthetic AβO$_{42}$. Reactivity to both anti-AβO^{cSNK} and 6E10 showed that APP23 brain-derived AβOs, including AβO^{cSNK}, were resistant to incubation with 1% SDS but susceptible to the combination of 1% SDS and boiling (Figure 4b). From these experiments, we surmise that synthetic and *ex vivo* brain-derived AβO^{cSNK} are not identical, suggesting an increase of denaturant stability of brain-derived AβO^{cSNK}.

Immuno-electron microscopy indicates that synthetic AβO^{cSNK} are spherical structures of varying size, 10−100 nm in diameter (Figure 4), similar to previous reports of AβO

DOI: 10.1021/acschemneuro.7b00469
ACS Chem. Neurosci. 2018, 9, 1591−1606

morphology.[27,39] This apparent size is inflated compared to the heights reported by our AFM analysis of AβO$_{42}$ (Supporting Figure 2a) as well as other AFM studies of AβOs,[49,50] perhaps as a result of drying and flattening artifacts, but was consistent between all transmission electron microscope (TEM) experiments (Figures 4 and 5 and Supporting Figure 3b). Notably, while 6E10 indiscriminately bound to both AβOs and fibrils, anti-AβO^{cSNK} binding was restricted to small oligomeric spherical structures (Figure 4**c**), and was not detected on morphological fibrils (Figure 4d). It is likely that solvent exposure of the Lys28 side chain confers specificity for AβO^{cSNK} in this context (Figures 1−3). In Aβ fibrils, the Lys28 side chain is oriented internally, stabilizing the fibril with a salt bridge to Asp23[30] (Figure 1a), and is not accessible to antibody recognition.

The antiserum A11, reactive to a generic β-sheet structure found in many protein aggregates,[17,18] as well as some natively folded proteins,[51] is often used as an oligomer specific antibody. Unlike A11, anti-AβO^{cSNK} is Aβ sequence and conformation specific (Supporting Figure 2b and Figure 3d).

We were also able to characterize synthetic AβO^{cSNK} biogenesis and maturation using immuno-electron microscopy. Appreciable AβO profiles were evident in Aβ_{42} monomer film reconstitutions after 6−8 h of incubation at 4 °C (Figure 4e), similar to previous reports.[27] The morphology of AβO^{cSNK}, indicated by gold labels after anti-AβO^{cSNK} binding, changed between 8 and 24 h; both the diameter range of AβO^{cSNK} and the number of anti-AβO^{cSNK} gold particles per AβO^{cSNK} was highest at 8 h and declined significantly by 24 h (Figure 4f−h). This may be due to enhanced packing and stability of AβOs mediated by internalization of the immunologically dominant Lys side chain of the cSNK epitope. Unlabeled oligomers (for example, Figure 4c) were excluded from this analysis. Recognizable fibrils did not form in the 24 h time course at 4 °C.

cSNK Is Involved in Aβ_{42} Aggregation. We investigated the role of cSNK in aggregation using immuno-electron microscopy. When anti-AβO^{cSNK} was added to Aβ monomer film reconstitution media, the maturation of all Aβ_{42} oligomers into smaller diameter forms was significantly delayed (Figure 5a). These data indicate that the cSNK epitope may be involved in templated aggregation and that antibody binding inhibits peptide−peptide interaction through cSNK. Alternately, the process of AβO maturation *in vitro* may be driven by internalization of the Lys28 side chain, which might be retained on the AβO surface in the presence of anti-AβO^{cSNK}.

Orthogonal validation for an active role of cSNK in Aβ aggregation was provided by a Thioflavin T (ThioT) assay, wherein the accumulation of β-sheet structure at room temperature over time is determined by increased fluorescence signal. Aβ_{42} monomer was reconstituted in the presence of decreasing molar ratios of anti-AβO^{cSNK} and control IgG1, 5:1−100:1 Aβ/antibody (Figure 5b, 5:1 ratio shown). We conducted a repeated measure analysis of variance (RM-ANOVA) to test for variation between the different molar ratios and treatments. We found that molar ratios of 50:1 and 100:1 Aβ/antibody had no effect on the accumulation of β-sheet content in the assay. However, at higher but still substoichiometric 5:1 and 10:1 Aβ/antibody molar ratios, anti-AβO^{cSNK} β-sheet accumulation was significantly reduced from Aβ_{42} alone (p = 0.0001) and from Aβ_{42} incubated with a negative control IgG1 (p = 0.0001). In contrast, Aβ_{42} incubated with negative control IgG1 was not significantly different from Aβ_{42} alone (p = 0.644).

To pinpoint the Aβ_{42} aggregation phase that was most affected by the anti-AβO^{cSNK} antibody, we calculated the lag phase rate, the elongation rate, and the maximum β-sheet signal for Aβ_{42} alone and with anti-AβO^{cSNK} or IgG1 for each of the molar ratios.[52,53] Again, the higher ratios of 50:1 and 100:1 Aβ/antibody were not significantly different in any of these measures from Aβ_{42} alone (Figure 5c−e). The difference between signals of Aβ_{42} alone and with anti-AβO^{cSNK} and control antibody were calculated, and data are presented as the fold change of the Aβ with antibody compared to the Aβ alone. Compared to Aβ_{42} monomer alone, anti-AβO^{cSNK} antibody delays the lag phase of β-sheet accumulation by ∼1.75-fold at 5:1 and 10:1 Aβ/antibody ratio (p < 0.0001, Figure 5c). This effect was statistically significant compared to IgG1 isotype control (p < 0.01), which has a non-statistically significant increase in lag phase compared to Aβ_{42} monomer alone (Figure 5b,c). The elongation rate showed a nonsignificant decrease, ∼0.5-fold, after incubation with anti-AβO^{cSNK} antibody at 5:1 and 10:1 ratios (p < 0.5, Figure 5d). The total β-sheet accumulated, as observed in the plateau phase, was significantly reduced by ∼0.25-fold with anti-AβO^{cSNK} antibody (5:1 ratio) compared to Aβ_{42} alone and the IgG1 isotype control (both comparisons p < 0.05, Figure 5e). This reduction in maximal β-sheet plateau suggests that the antibody is binding and stabilizing Aβ in its oligomeric, low β-sheet containing conformation, preventing a minority of Aβ from converting to high β-sheet containing fibrils. This was confirmed by TEM imaging (Supporting Figure 3b); by 30 h, oligomers are rarely observed in the Aβ_{42} sample, corresponding to the elongation phase, and only sparsely observed at 48 and 72 h, the plateau phase. In contrast, if Aβ_{42} is incubated with anti-AβO^{cSNK}, oligomers are readily found at 48 h, the beginning of the plateau phase; by 72 h, oligomers are sparsely observed (Supporting Figure 3b). Similarly, when the presence of soluble versus insoluble aggregates in the assay was investigated through the time course, it was clear that anti-AβO^{cSNK} delays the formation of insoluble aggregates by at least 20 h (Supporting Figure 3).

These TEM and ThioT analyses indicate that anti-AβO^{cSNK} inhibits the aggregation of Aβ polymers *in vitro,* displaying its most prominent effects in early stages. In the lag phase as monomers begin to form oligomers, the cSNK epitope is exposed and is subsequently bound by anti-AβO^{cSNK}. This binding slows the accumulation of β-sheet and oligomeric structures; likewise, this blockade slows the transition from oligomers to fibrils as the majority species in the population. However, once a critical concentration of oligomers (including protofibrils) has been reached, the elongation phase begins, in which fibrils recruit monomer at a faster rate than oligomers.[54] Thus, in the elongation phase, anti-AβO^{cSNK} has a reduced impact because fibrils do not display the cSNK epitope. Finally, a significant reduction in plateau β-sheet structure suggests that, by maintaining some structures in an oligomeric form, the anti-AβO^{cSNK} antibody has a negative downstream effect on total Aβ fibril content *in vitro* and perhaps even *in vivo* (Supporting Figure 5b).

AβO^{cSNK} Is Present in Human Alzheimer's Disease Brain and Cerebrospinal Fluid (CSF) and Absent from Human Brain Fibrillar Aβ Plaques. To determine if AβO^{cSNK} contributes to the AβO population in humans, we probed human brain tissues obtained from AD and age matched control individuals with the anti-AβO^{cSNK} antibody. Brain (frontal cortex) extracts were generated with detergent-free Tris-buffered saline (TBS) to ensure integrity of the structured epitope after homogenization. Extracts were ultracentrifuged, and supernatants were analyzed to ensure that soluble oligomeric material was being evaluated. Surface plasmon resonance (SPR) assessment determined that anti-AβO^{cSNK} specifically recognized a soluble analyte present in

DOI: 10.1021/acschemneuro.7b00469
ACS Chem. Neurosci. 2018, 9, 1591−1606

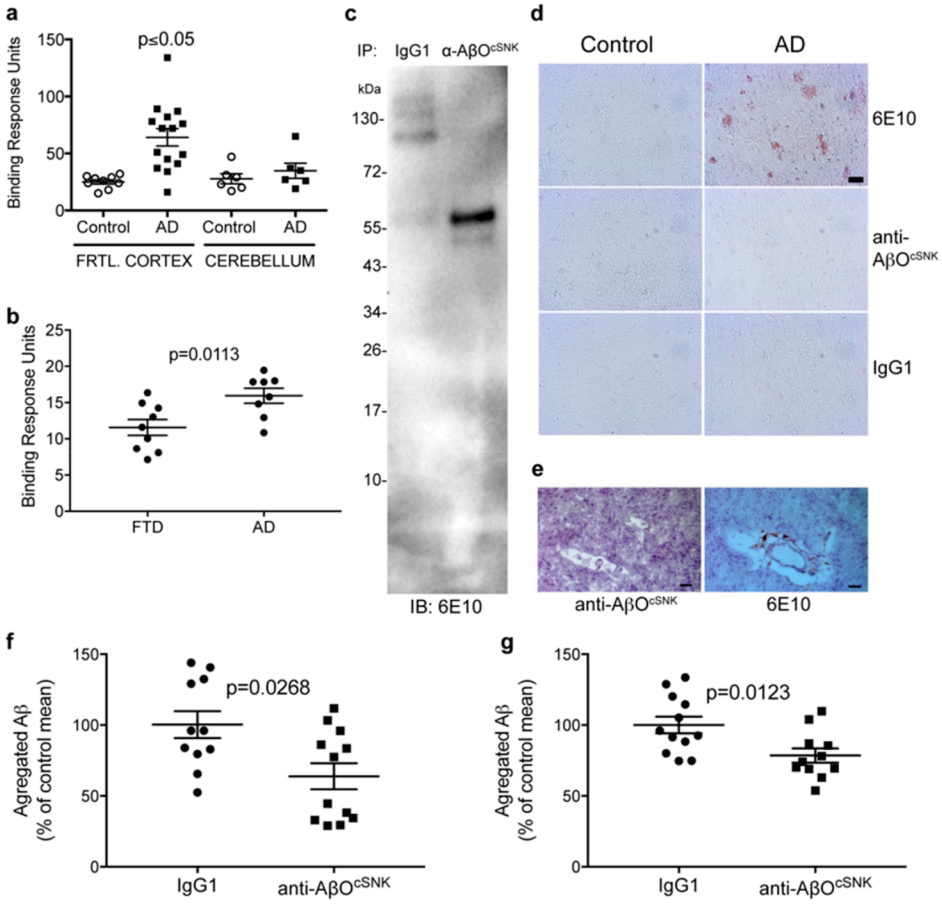

Figure 6. Anti-AβO^{cSNK} selectively recognizes a soluble molecular species in AD brain and CSF. (a) Binding response of AD and aged-matched control human brain homogenates from the frontal cortex (Frtl. Cortex) Brodmann 9 and the cerebellum to anti-AβO^{cSNK}. Data is normal, and binding differentials were determined by one-way ANOVA with Bonferroni post-test: frontal cortex control vs AD $p < 0.001$, frontal cortex AD vs cerebellum control $p < 0.01$, frontal cortex AD vs cerebellum AD $p < 0.05$. No other comparisons have significant differences. (b) Binding response of CSF from AD and aged matched frontotemporal dementia (FTD) patients to anti-AβO^{cSNK} ($p < 0.0113$, independent two-tailed t test). For panels a and b, each dot represents one individual; the binding was analyzed at least twice. Mean and SEM are shown. (c) Immunoprecipitation of human AD brain extract with anti-AβO^{cSNK} and IgG1 control antibody. Membrane was probed with pan-Aβ antibody 6E10. An AβO^{cSNK} specific Aβ band is evident at ~56 kDa. Results are representative of at least four independent experiments. (d, e) Sections from the frontal cortex of human AD and age matched control brain were stained with 1 μg/mL of 6E10, anti-AβO^{cSNK}, or an isotype control IgG1. Antibody labeling is shown in brown, and counterstaining with hematoxylin is shown in blue. The results are representative of four independent experiments with 8 different individuals (4 AD and 4 age matched controls). Scale is applicable to all images and = 50 μm. (e) Serial brain sections including a blood vessel from an AD, Braak VI patient. Scale bar = 50 μm. (f) AβO levels in Tg2576 (11 IgG1 treated mice and 12 anti-AβO^{cSNK} treated mice) and APP/PS1 (12 IgG1 treated mice and 11 anti-AβO^{cSNK} treated mice) animals expressed as a percentage of the mean of the IgG1 control treated animals after weekly dosing with anti-AβO^{cSNK} and IgG1 control. Mean and SEM is shown. Tg2576 differences do not pass Shapiro–Wilk normality test; Mann–Whitney two-tailed unpaired test defined p value. APP/PS1 differences are normal, determined by two-tailed unpaired t test.

human AD brain ($p \leq 0.05$, Figure 6a) and CSF ($p = 0.0113$, Figure 6b), while displaying negligible reactivity in healthy control samples or samples from patients with frontotemporal dementia. In addition, the detection of AβO^{cSNK} in CSF had a significant positive correlation with the total tau and phospho-tau levels in these same samples, as determined separately by INNOTEST ELISA (Table 1), indicating that AβO^{cSNK} tracks with biomarkers of neurodegeneration.[55,56] Furthermore, AβO^{cSNK} in CSF had no discernible correlation with total Aβ_{42}, suggesting that AβO^{cSNK} is not a passive marker of CSF Aβ_{42} concentration. Notably, little to no AβO^{cSNK} was detected in either AD or control brain cerebellum, a region of the brain that does not display typical Aβ neuritic plaque pathology or neurodegeneration (Figure 6a).[57]

AD brain extracts were subjected to immunoprecipitation with anti-AβO^{cSNK} and an IgG1 isotype control. Consistent with the AD brain and CSF SPR results, the anti-AβO^{cSNK} precipitate contained material reactive to anti-Aβ antibodies (Figure 6c). The dominant band, ~56 kDa in size, was not detected in the control IgG1 precipitates. Notably, human brain AβO^{cSNK} is at least partially SDS-resistant, as the signal was detected after SDS-PAGE (Figure 6c). This finding is consistent with our examination of AβO^{cSNK} from APP/PS1 mouse brain extracts,

Table 1. AβO^{cSNK} in CSF Is Correlated with Tau Levels[a]

	total Aβ_{1-42}	total tau	p-181 tau
Pearson correlation	−0.245	0.548[c]	0.635[c]
p value ≤ (2-tailed)	0.297	0.012[c]	0.003[c]
N[b]	20	20	20

[a]Levels of AβO^{cSNK} (oligomeric Aβ, cSNK-reactive) in the CSF of human AD and non-AD patients as determined by SPR were correlated with levels of total Aβ_{1-42}, total tau, and phosphorylated tau from those same patients, as determined by ELISA. [b]Number of patients. [c]Statistically significant correlation.

DOI: 10.1021/acschemneuro.7b00469
ACS Chem. Neurosci. 2018, 9, 1591−1606

which were also SDS-resistant, in contrast to synthetic AβO^{cSNK} (Figure 3b), and again suggests that brain-derived AβO^{cSNK} have properties that differ from synthetic oligomers against which many "oligomer-specific" antibodies have been previously generated.

In our molecular dynamics work, we found no overlap between cSNK and Aβ fibril conformational ensembles (Figure 2a−d), and in biochemical studies, we found no reactivity of anti-AβO^{cSNK} to synthetic Aβ fibrils (Figure 3c,d). To confirm that the cSNK structured epitope is not displayed by native Aβ fibrils, we probed frontal cortex brain sections from AD and age-matched control subjects with anti-AβO^{cSNK}. In frozen sections, plaques are clearly detected by pan-Aβ 6E10 in AD brains, whereas anti-AβO^{cSNK}-probed sections show an absence of signal (Figure 6d), indicating that fibrillar Aβ lacks the cSNK surface epitope, and that antibodies targeting this epitope are incapable of recognizing Aβ fibrils. This finding was confirmed with brain sections from aged APP/PS1 mice (Supporting Figure 2d). Moreover, we see no anti-AβO^{cSNK} reactivity to vascular amyloid deposits in human brains (Figure 6e).

AβO^{cSNK} Constitutes a Minority of AβOs in Brains of Aged AD Mouse Models. AβOs are polymorphic, occurring in sizes ranging from 8 kDa dimers to 150 kDa oligomers, and these different sizes have been reported to evolve in relative concentration in the brain during the course of disease, yielding varying synapto- and behavioral toxicities.[6,58−62] The identification of the cSNK AβO-specific epitope provides a unique tool for the immunological classification of AβOs and their selective toxicities in AD, allowing for the detection and manipulation *in vivo* of a particular Aβ assembly, AβO^{cSNK}.

To determine the relative contribution of AβO^{cSNK} to the entire population of AβOs in the brain we designed an *in vivo* "immuno-depletion" experiment to specifically clear AβO^{cSNK} and then quantify the total remaining AβO using the A4 physicochemical test.[63] This unbiased test collects soluble aggregated Aβ, then performs a deaggregating step, resulting in a homogeneous population of essentially monomeric Aβ. Finally the absorbance of monomerized brain homogenate derived Aβ at 570 nm is compared to an $Aβ_{40}$ standard curve.[63] Given the fact that oligomers are transient and plastic,[64] any reduction of total AβO *in vivo* upon specific AβO^{cSNK} targeting may be net of the presumably rapid generation and interconversion of AβO subclasses in these animal models.

Twelve month-old male Tg2576 and APP/PS1 mice were intraperitoneally injected weekly with 30 mg/kg of anti-AβO^{cSNK} for 6 weeks. In both mouse models, anti-AβO^{cSNK} treated animals had significantly lower levels of soluble Aβ aggregates in saline brain extracts compared to IgG1 treated controls (30% and 20% reduction, $p = 0.012$ and $p = 0.012$, respective, Figure 6f). This indicates that 20−30% of the total brain AβO population can form AβO^{cSNK} and are thus sensitive to engagement by anti-AβO^{cSNK} and subsequent clearance. Notably, the murine IgG1 Fc subclass of the anti-AβO^{cSNK} monoclonal antibody necessitates that clearance occur without the participation of Fc receptor-bearing brain cells, such as microglia.

AβO^{cSNK} Mediate Behavioral Toxicity *in Vivo* in WT and AD Mice. We used an *in vivo* model of acute AβO toxicity, wherein intracerebroventricular (ICV) injections of synthetic $AβO_{42}$ into wild-type (WT) mice induce significant impairment in the novel object recognition memory task,[4] to determine if AβO^{cSNK} contributes to the toxicity observed with $AβO_{42}$. As expected, a significantly lower discrimination index, indicative of memory impairment, in mice treated with synthetic AβO42 when compared to vehicle-treated mice was observed (Figure 7a). Preincubation of 1 mM $AβO_{42}$ with 0.25 mM anti-AβO^{cSNK} for

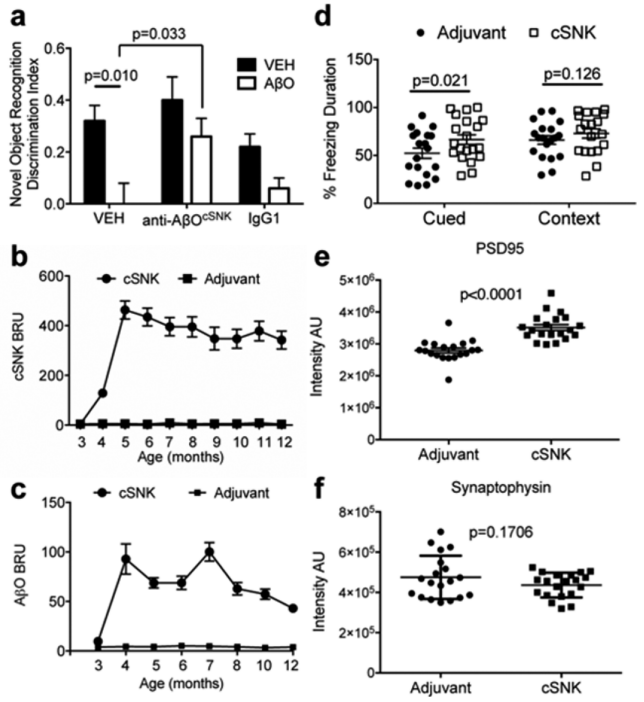

Figure 7. AβO^{cSNK} impairs memory, while induced polyclonal AβO^{cSNK}-specific immune response improves cued memory and PSD95 global expression. (a) NOR discrimination indices of wild-type mice injected with $AβO_{42}$ and either anti-AβO^{cSNK} or a mouse IgG1. $n = 5$ mice per control (VEH black bars) group, 15 mice per AβO (white bars) treated group. Differences were compared using ANOVA with Bonferroni post-test. (b−f) APP/PS1 mice were vaccinated with either cSNK-KLH or adjuvant alone. (b) Anti-cSNK titer levels in plasma from vaccinated mice. Data points represent 38 (3−6 months), 34 (6−7 months), 30 (8−9 months), and 26 (10−12 months) mice. (c) Binding response to $AβO_{42}$ over the course of immunization. Results from 12 randomly selected cSNK vaccinated mice are shown. BRU: binding response units. (d) Cued (% Freezing Duration during tone presentation) and contextual (% Freezing Duration across 5 min of testing) fear conditioning test of vaccinated animals at 11 months of age. Differences were determined using a multivariate regression model (see Table 2). (e, f) Hemibrains were homogenized in saline and soluble extracts analyzed for global PSD95 (e) and synaptophysin (f) expression by immunoblotting. Means from five immunoblotting replicates are shown. Differences were analyzed by Shapiro−Wilk and were not normal; p values determined with a Mann−Whitney two-tailed unpaired test. Nineteen adjuvant treated mice and 20 cSNK treated mice are included in the analyses for panels d−f. Mean and SEM are shown throughout.

1 h resulted in significant antagonism of $AβO_{42}$-induced behavioral toxicity ($p = 0.033$ compared to $AβO_{42}$ alone). The memory performance of the anti-AβO^{cSNK} treated mice was comparable to that of vehicle-treated mice ($p = 0.989$, Figure 7a). We conclude that the $AβO_{42}$ injection material includes AβO^{cSNK} structures that impair memory in WT mice, which can be blocked by the anti-AβO^{cSNK} antibody. In light of our earlier finding that AβO^{cSNK} constitutes a minority of total synthetic AβO (Figure 6f), the behavioral protection provided by the antibody when injected along with $AβO_{42}$ (Figure 7a) suggests that AβO^{cSNK} are preferentially toxic in this system. Again, the virtually complete abrogation of behavioral toxicity with the IgG1 anti-AβO^{cSNK} antibody suggests that simple neutralization

DOI: 10.1021/acschemneuro.7b00469
ACS Chem. Neurosci. 2018, 9, 1591−1606

effected the observed behavioral amelioration, rather than microglial clearance of immune complexes. Crucially, infusion of anti-AβO^{cSNK} or isotype control IgG1 alone did not impact memory (Figure 7a), consistent with anti-AβO^{cSNK} not recognizing functionally important proteins in the WT mouse brain.

Defining pathogenic activities of AβO subclasses *in vivo* is a long-sought goal of the field.[65] To investigate the pathogenesis of AβO^{cSNK} through the course of the disease, we vaccinated young APP/PS1 mice against the cSNK epitope and followed those animals through presentation of advanced disease at 13 months of age. The cSNK immunization induced a robust anti-cSNK humoral response (Figure 7b), while anti-cSNK titers for baseline plasma (month 3) and adjuvant treated animals were negligible. The anti-cSNK humoral response was reflective of an anti-AβO^{cSNK} response, as plasma from cSNK-immunized mice had strong reactivity to synthetic $AβO_{42}$ (Figure 7c). The polyclonal anti-AβO^{cSNK} immunoglobulins were predominantly of the Fc-functionless mouse IgG1 subclass (Supporting Figure 4a). Antigenic spread to fibril determinants in the polyclonal anti-AβO^{cSNK} response was excluded (Supporting Figure 4b), and reactivity to monomeric Aβ was minimal (Supporting Figure 4c).

Behavioral, biochemical, and morphological assessments were conducted on immunized mice. We built a multivariate regression model to test the significance of the outcome measures, with sex and treatment encompassing the multiple variables (Table 2).

Table 2. Primary Outcomes and Significance from cSNK Vaccination in APP/PS1 Mice[a]

	fear conditioning			ThioS plaque area (%)	
	cued	context	AβO levels in brain	cortex	hippocampus
sex	0.014[b]	0.008[b]	0.002[b]	0.084	0.010[b]
treatment	0.021[b]	0.126	0.290	0.077	0.484

[a]APP/PS1 mice were vaccinated with cSNK or adjuvant alone. Primary outcomes are listed. Differences between treatments and sexes were tested using a regression model with categorical covariates (ANOVA) using XLSTAT V2014.6.04; *p* values are shown. [b]Statistically significant value.

Sex was found to be a significant variable for most outcome measures (Table 2). It is well documented that AD disproportionately affects women in both prevalence and severity[66] and female AD mouse models are known to display higher amyloid plaque burden than males;[67] however, the biologic mechanisms underlying these sex differences are not fully understood.[68]

The polyclonal anti-AβO^{cSNK} immune response was significantly associated with improved emotional memory, measured by the cued fear conditioning (FC) task ($p = 0.021$, Table 2 and Figure 7d). In contrast, spatial memory was not changed by cSNK immunization, measured in the contextual FC task ($p = 0.126$, Figure 7d). Postsynaptic dendritic spines in young AD mice are particularly sensitive to AβO toxicity.[69−71] We found that cSNK vaccination significantly preserved global concentration of the postsynaptic marker PSD95 (Figure 7e), in comparison to mice immunized with adjuvant alone. Levels of presynaptic marker synaptophysin were unchanged by cSNK vaccination (Figure 7f). This pattern is consistent with previous work investigating Aβ pathology.[71] Soluble AβO levels in brain extracts were reduced approximately 15% by cSNK vaccination, though this effect did not reach statistical significance ($p = 0.0783$, Supporting Figure 5a).

From the perspective of *in vivo* antibody subtraction, these results suggest that antibody-accessible brain AβO^{cSNK}, a minority of total brain AβO (Figure 6f), participates substantially in the postsynaptic impairment observed in AD and mouse models of the disease and that antibody binding of AβO^{cSNK} may inhibit the accumulation of fibril plaques over time. Furthermore, a locally mediated activity of endogenous AβO^{cSNK} includes significant fear conditioning memory impairment.

The immunodepletion approach also reveals that AβO^{cSNK} plays a minor role in global plaque deposition *in vivo*. A humoral response against AβO^{cSNK} only slightly reduces the total β-sheet plaque accumulated in the cortex (Supporting Figure 5b, cortex $p = 0.084$, hippocampus, $p = 0.484$), suggesting that AβO^{cSNK} are generally not intermediates or fragmentation products of Aβ fibrils, as reputed by some AβO classes, such as protofibrils.[19,46] That any reduction is evident is not because AβO^{cSNK} are fibril precursors but because binding of AβO by anti-AβO^{cSNK} stabilizes the oligomer structure, preventing its recruitment into higher β-sheet structures. This is also supported by the *in vitro* aggregation study, which shows that anti-AβO^{cSNK} (1) blocks formation of soluble oligomers from monomers, (2) has a nonsignificant effect on elongation of fibrils, and (3) reduces the maximal β-sheet produced (Figure 5). These *in vivo* and *in vitro* studies allow us to conclude that the anti-AβO^{cSNK} inhibits the oligomer−fibril transition of the Aβ population at large.[53]

CONCLUSION

We have identified a class of toxic AβOs, AβO^{cSNK}, defined by their conformational presentation of three immunogenic Aβ residues in a constrained turn epitope (cSNK). Solvent exposure of the Lys28 side chain and constrained turn configuration confers specificity for AβO^{cSNK}. Utilizing an *in vivo* immunodepletion strategy, we show that AβO^{cSNK} participate in behavioral toxicity and postsynaptic impairment. Our *in vivo* and *in vitro* studies suggest that anti-AβO^{cSNK} inhibits the oligomer-fibril transition of Aβ, while neutralizing the toxic activity of AβOs.

At least some AβO subclasses propagate according to their initial structures. Indeed, some of the clinical diversity of AD may be determined by AβO prion-like strains.[72] It is intriguing to consider that a number of quasi-stable strains of AβOs might be implicated in the clinical phenomenology of AD patients, and immunologic phenotyping may be able to meaningfully deconvolute AβO subtypes with specific pathogenic activities in AD.

MATERIALS AND METHODS

Molecular Dynamics Simulations. Cyclic peptides of amino acid sequences (1) CGSNKGG and (2) CGSNKGC were constructed for equilibrium simulations. These peptides include flanking amino acids that were covalently bonded by either a peptide bond between N-terminal C and C-terminal G for peptide 1 or by a disulfide bond between cysteine side chains for peptide 2. Equilibrium simulations on these cyclic peptides were performed for 500 ns using the CHARMM27 force field[73,74] in explicit TIP3P water[75] with 100 mM NaCl. Analysis was performed on 15000 configurations taken in equally spaced time intervals between 10 and 500 ns. Simulations of $Aβ_{42}$ monomer are performed as follows: Starting from a PDB structure of $Aβ_{42}$ monomer (1Z0Q), we generated 6000 different configurations using a Pivot-crankshaft combined movement method;[76] we then performed a 3 ns equilibrium simulation for each of these 6000 configurations in CHARMM22*[77] with explicit TIP3P water with 100 mM NaCl. The analysis was performed on the final equilibrated configurations from these 6000 3 ns simulations. The ensemble-averaged solvent-accessible surface area (SASA)[44,45] of the amino acid side chains was obtained using a probe with water radius 1.4 Å.

The Aβ fibril structure was taken from PDB structure 2M4J.[43] A 35 ns equilibrium simulation of the structure 2M4J was performed using the

DOI: 10.1021/acschemneuro.7b00469
ACS Chem. Neurosci. 2018, 9, 1591−1606

CHARMM27 force field in TIP3P solvent with 100 mM NaCl, from which 10000 configurations were taken for analysis. The fibril structure consists of 9 chains in the form of a 3-fold symmetric trimer, which is stacked 3 chains deep. To avoid fibril end-cap artifacts, we only analyzed the middle chains of this structure. Additionally, we only analyzed the heavy (non-hydrogen) atoms in the sequence SNKG in each of these chains. RMSD clustering was performed using the maxcluster algorithm (http://www.sbg.bio.ic.ac.uk/maxcluster). Three RMSD values are obtained by aligning all heavy atoms in the segment (SNKG) in each sampled conformation to three different reference structures, which consist of the centroid of the cyclic peptide ensemble, the centroid of the monomeric $A\beta_{42}$ ensemble, and the centroid of the 2M4J fibril ensemble. These three RMSD values are then plotted in a three-dimensional scatter plot. The fraction (percent) of the monomeric $A\beta_{42}$ ensemble that overlaps with the cyclic peptide ensemble is obtained by first dividing the volume of this three-dimensional RMSD space up into cubic elements of length 0.1 Å. A threshold or cutoff density for the points in the cyclic distribution is then determined such that the cubes with cyclic distribution density equal to or higher than the cutoff density contain 90% of the points in the cyclic distribution. This defines a volume (which may be discontinuous) that gives the characteristic volume containing the cyclic distribution and removes any artifacts due to outliers. The fractions of points from the linear monomeric distribution and fibril ensembles within this volume are directly counted, to define the degree of structural overlap between the two ensembles as a percentage.

Peptide Synthesis. Two distinct cyclic peptides comprising the cSNK epitope were constructed using the native Aβ sequence GSNKG.

The c[CGSNKGC] peptide synthesis for exploratory antibody generation was performed by CPC Scientific Inc. (Sunnyvale CA, USA) following standard manufacturing procedures and included a poly-(ethylene glycol) (PEG2) addition to the N terminal cysteine. Peptide sequence was confirmed by electrospray mass spectral analysis and observed to have the predicted molecular weight, 811.2 g/mol. Purity was assessed by HPLC with a SepaxGP-C18 column and was determined to be 95%. Cyclization was performed via a Cys−Cys side chain-to-side chain disulfide bridge. c[CGSNKGC-PEG2] was then conjugated to either KLH or BSA via a maleimide-based coupling using maleimide-BSA.

Noncyclized, linear CGSNKGC-PEG2 peptide was also produced by CPC Scientific. Electrospray mass spectral analysis showed the [CGSNKGC-PEG2] to have a molecular weight of 813.2 g/mol, 2 g/mol higher than the cyclic peptide, consistent with the extra hydrogens associated with the linear peptide. The purity determined by HPLC was 95.5%.

The c[CGSNKGG] peptide was generated by JPT Peptide Technologies (Acton MA, USA), and a head-to-tail (C-to-G) amide bond cyclization was performed along with maleimide-based conjugation to KLH. The thiol provided by the N terminal cysteine was chemoselectively coupled to the maleimide modified KLH. Free peptide was removed by dialysis. Sequence confirmation by electrospray ionization mass spectrometry determined the peptide to be of the predicted molecular weight, 603.7 g/mol. HPLC with a 220 nm C18 linear gradient confirmed a greater than 95.7% purity; a peak corresponding with noncyclized peptide, see below, represented less than 5% of the sample. The peptide was provided as a trifluoroacetate salt.

JPT Peptide Technologies also produced a noncyclized CGSNKGG. Electrospray mass spectral analysis showed the CGSNKGG to have a molecular weight of 621.7 g/mol, 18 g/mol higher than the cyclic peptide, consistent with the extra oxygen and hydrogens associated with the linear peptide. The purity determined by HPLC was 95.7%.

Antibody Generation and Selection. The Cys−Cys cSNK peptide was linked to keyhole limpet hemocyanin (KLH), as previously done for prion protein (PrP) and superoxide dismutase 1 (SOD1)-misfolding specific epitopes.[78,79] The peptides were used by Immunoprecise Antibodies LTD (Victoria BC, Canada) for mouse monoclonal antibody production, following protocols approved by the Canadian Council on Animal Care. Mouse sera were screened, by Immunoprecise, on the GSNKG-peptide linked to BSA. Positive IgG-secreting clones were subjected to large-scale production.

Monoclonal antibodies were captured from tissue culture supernatants using a rabbit anti-mouse Fc-specific (RAMFc) antibody (Sigma-Aldrich Canada Co., Oakville, ON, Canada), which was covalently immobilized on a CM5 sensor chip (GE Healthcare - Biacore Life Sciences, Pittsburgh, PA, USA).

Binding of the lead clone, anti-$A\beta O^{cSNK}$, to linear and cyclic SNK peptides conjugated to BSA was examined using a Biacore 3000 instrument (GE Healthcare). For affinity analysis, cSNK−BSA and BSA were immobilized at low densities (50−100 RU) on adjacent flow cells. Serial 2-fold dilutions of anti-$A\beta O^{cSNK}$ (4.7 nM to 75 nM) were then sequentially injected over the surfaces at 60 μL/min for 3 min, followed by a dissociation phase. Sensorgrams were double-reference subtracted and fitted to a Langmuir 1:1 binding model. Three separate analyses were performed on three consecutive days using the same sensor chip and the same conditions.

Aβ Oligomerization and Characterization. Recombinant $A\beta_{40}$ and $A\beta_{42}$ peptides (California Peptide, Salt Lake City UT, USA) were dissolved in ice-cold hexafluoroisopropanol (HFIP). The HFIP was removed by evaporation overnight and dried in a SpeedVac centrifuge. To prepare monomers, the peptide film was reconstituted in DMSO to 5 mM, diluted further to 100 μM in dH_2O, and used immediately. Oligomers were prepared by diluting the 5 mM DMSO peptide solution in phenol red-free F12 medium (Life Technologies Inc., Burlington ON, Canada) to a final concentration of 100 μM and incubated for 1−7 days at 4 °C unless otherwise noted. Scrambled $A\beta_{42}$ peptide controls (rPeptide, Bogart GA, USA) were prepared under similar conditions.

$A\beta_{42}$ oligomers, monomers, and BSA were covalently coupled on separate flow cells of two CM5 sensor chips at a concentration of 3500−4000 response units. BSA was similarly immobilized to serve as a reference surface. Antibodies anti-$A\beta O^{cSNK}$, 6E10 (Covance, Montreal QC, Canada), and mouse IgG1 isotype control (Abcam, Toronto ON, Canada) were diluted and sequentially injected over the surfaces. Binding responses were monitored in real time and report points collected in the dissociation phase of the sensorgram.

Binding of Anti-$A\beta O^{cSNK}$ to Scrambled Aβ Oligomers. Approximately 1050 RUs of $A\beta_{1-42}$ oligomers and scrambled $A\beta_{1-42}$ oligomers were immobilized on separate flow cells of a CM5 sensor chip. A reference surface was created by activating and blocking an adjacent flow cell. Anti-$A\beta O^{cSNK}$, diluted to 1 μM in 4-(2-hydroxyethyl)-1-piperazineethanesulfonic acid (HEPES) buffered saline (HBS) containing 0.05% p20 surfactant and 1 mg/mL carboxymethyl dextran (CMD), was then injected over all flow cells at 20 μL/min and allowed to associate with the oligomers and reference surface for 180 s. Running buffer (HBS) was then injected for 150 s to observe dissociation. Resultant sensorgrams were double-referenced by subtracting binding responses on the reference surface and buffer blanks.

Immunoblotting. For dot blotting, stated amounts of protein were dotted directly onto 0.45 μm nitrocellulose membranes (Pall Corporation, Mississauga, ON, Canada). For SDS-PAGE, equal amounts of protein were fractionated by Tris-glycine 4−20% gels after boiling or not in Tris-glycine sample buffer and transferred to 0.2 μm poly(vinylidene difluoride) (PVDF) membranes. Antibodies used include 6E10 (Biolegend), PSD95 (Abcam), synaptophysin (Abcam), and anti-$A\beta O^{cSNK}$.

Immuno-gold Labeling for Transmission Electron Microscopy. Aβ oligomer or fibril preparation (0.5 μL of 100 μM) was diluted in 2 μL of filtered distilled water, spotted onto Formvar-coated 200-mesh nickel grids (EM Sciences), and allowed to dry. Two microliters of goat serum was used as a soluble protein control. Grids were blocked for 2 × 10 min in 1% milk in PBS, incubated in primary antibody in 1% milk in PBS (anti-$A\beta O^{cSNK}$ at 1 mg/mL, 6E10 at 25 μg/mL, or block only for negative control) for 2 h at room temperature, washed in PBS, incubated in anti-mouse secondary antibody conjugated to 10 nm gold beads (1:30, EM Sciences) in 1% milk PBS with 0.05% polyethylene glycol for 1 h at room temperature, washed in PBS, washed in several changes of filtered distilled water, and allowed to dry. Grids were then negatively stained with 0.5% aqueous uranyl acetate for 30 s, and viewed on a FEI Tecnai G2 spirit transmission electron microscope.

Quantification of AβO Diameter and Anti-$A\beta O^{cSNK}$ Reactivity. For the time course of formation of $A\beta O^{cSNK}$, grids containing $A\beta O_{42}$ that

DOI: 10.1021/acschemneuro.7b00469
ACS Chem. Neurosci. 2018, 9, 1591−1606

had been allowed to form for 8, 10, 12, or 24 h were fixed and labeled for anti-AβO^{cSNK} as above. Sampling of grids was performed in an unbiased manner by working from the center in a spiral, and photographing the first 40 fields that contained AβO$_{42}$. File names were then coded so that the experimenter was blinded to condition. For each image, every AβO^{cSNK} visible was scored for number of gold beads and diameter, measured using ImageJ.

For inhibition of AβO$_{42}$ formation, Aβ_{1-42} peptide was incubated at 4 °C for oligomer formation (as above) in the presence of 9.8 mg/mL anti-AβO^{cSNK} antibody or IgG1 control, for a range of times. AβO$_{42}$ was then spotted onto grids and counterstained with uranyl acetate. Sampling of grids was performed in an unbiased manner as above. File names were blinded, and diameter of AβO$_{42}$ was measured as above. For both analyses, the data presented represents one biological replicate. A second biological replicate was performed in each case and confirmed to give similar results.

Thioflavin T β-Sheet Aggregation Assay. HFIP-treated amyloid-β peptides (BACHEM, no. H-7442) were resuspended in 10 mM NaOH to a concentration of 500 μM, sonicated for 10 min, and then diluted to 50 μM in 1 mM ethylenediaminetetraacetic acid (EDTA) Tris-HCl buffer. They were then immediately added to a black walled 96-well plate either with buffer alone or with decreasing amounts of either IgG1 isotype control or anti-AβO^{cSNK} at molar ratios of 5:1, 10:1, 50:1 or 100:1 Aβ to antibody, for a final volume of 100 μL. Assay controls included buffer alone and antibody only, and treatment groups were tested in duplicate. Thioflavin T (10 μM final) was incubated with sample at room temperature for 72 h, and readings were taken every hour at 440 nm excitation and 485 nm emission. We ran a repeated measure analysis of variance (RM-ANOVA) to test for variation between the different molar ratios and treatments. Values of $p < 0.05$ were considered significant. SPSS V24 was used for statistical analysis.

The data was fitted with Boltzmann sigmoidal curves on GraphPad Prism 6.0 with $R^2 > 0.85$, and the maximum detected fluorescence (F_f), the initial fluorescence value (F_i), the gradient of the curve (k), and t_{50} (the midpoint between F_i and F_f) were used to calculate the lag phase duration and the elongation rate, following methods previously described.[52]

Elongation rate:

$$\frac{(F_f - F_i)}{4k}$$

Lag Phase:

$$t_{lag} = \frac{4kF_i}{(F_f - F_i)} + t_{50} - \{2k\}$$

Results were plotted relative to the values found for Aβ alone, as a ratio where values above 1 signify an increase.

Human Tissues and Analyses. Human brain tissues were obtained from the University of Maryland Brain and Tissue Bank upon approval from the UBC Clinical Research Ethics Board (C04-0595). CSF samples were obtained from patients assessed at the UBC Hospital Clinic for Alzheimer's and Related Disorders. The study was approved by the UBC Clinical Research Ethics Board, and written consent from the participant or legal next of kin was obtained prior to collection of CSF samples. Clinical diagnosis of probable AD was based on NINCDS-ADRDA criteria.[80] CSF samples were collected in polypropylene tubes, processed, aliquoted into 100 μL polypropylene vials, and stored at −80 °C within 1 h after lumbar puncture.

Homogenization. Human and APP23 mouse brain tissue samples were weighed and subsequently submersed in a volume of fresh, ice cold TBS (supplemented with 5 mM ethylene glycol-bis(β-aminoethyl ether)-*N*,*N*,*N*′,*N*′-tetraacetic acid (EGTA), 5 mM EDTA, (both from Sigma), and EDTA-free protease inhibitor cocktail from Roche Diagnostics, Laval QC, Canada) such that the final concentration of brain tissue was 20% (w/v). Tissue was homogenized in this buffer using a mechanical probe homogenizer (3 × 30 s pulses with 30 s pauses between pulses, all performed on ice). TBS homogenized samples were then subjected to ultracentrifugation (70 000*g* for 90 min). Supernatants were collected, aliquoted, and stored at −80 °C. The protein concentration of TBS homogenates was determined using a BCA protein assay (Pierce Biotechnology Inc., Rockford IL, USA).

Surface Plasmon Resonance Analysis. Twenty CSF samples and 34 brains from AD patients and age-matched controls were analyzed. Brain samples, homogenized in TBS, included frontal cortex Brodmann area 9 (n = 24) and, in some cases, the corresponding cerebellum (n = 9). Anti-AβO^{cSNK} and an IgG1 isotype control were directly immobilized at high densities (~10 000 RU) on 2 separate flow cells of a sensor chip. Using a Biacore 3000, diluted samples were injected sequentially over the surfaces for 300 s, followed by 150 s of dissociation in buffer and surface regeneration. Binding responses were double-referenced by subtraction of IgG1 reference surface binding and normalized with assay buffer, and the different groups of samples were compared.

Aβ_{1-42}, Total Tau, and Phospho-tau ELISA. CSF Aβ_{1-42}, total tau, and 191-phosphorylated tau were measured in duplicate using commercial ELISA assay kits according to manufacturer's protocol (INNOTEST ELISAs, Innogenetics, Gent, Belgium). The plates were read with a SpectraMax Plus spectrophotometer (VWR, Radnor, PA, USA), and calibration curves were generated by SOFTmax.RTM PRO software.

Immunoprecipitation. Immunoprecipitation was performed with the Dynabead Co-Immunoprecipitation Kit (LifeTechnologies) following the manufacturer's instructions. Briefly, 2.5 g of human brain was subjected to cryolysis using the Cellcrusher (Cellcrusher, Portland, OR, USA) followed by homogenization in TBS plus protease inhibitor. Five milligrams of antibody coupled beads (with 10 mg/mL coupled antibody) were used to immunoprecipitate the human brain extract. After elution from the beads, bound proteins were lyophilized overnight and analyzed by SDS-PAGE and immunoblotting.

Immunohistochemistry. Immunohistochemistry was performed on frozen human brain sections, post-fixed in 10% formalin or unfixed. Endogenous peroxidase activity was quenched using 0.5% hydrogen peroxide in methanol for 20 min. Antigen retrieval was performed on some slides, using sodium citrate, pH 6.0, and steam heating for 25 min followed by cooling at room temperature (RT) for 30 min. After stabilization in TBS for 5−7 min, sections were treated with 70% formic acid for 15 min at RT, and then washed 3 × 15 min in TBS. In a humidified chamber, nonspecific staining was blocked by incubation with serum-free protein blocking reagent (Dako Canada Inc., Mississauga, ON, Canada) for 1 h. For immunostaining, anti-AβO^{cSNK} (1 μg/mL), 6E10 (1 μg/mL), and IgG1 (1 μg/mL, Abcam) were used as primary antibodies. Sections were incubated overnight at 4 °C and washed 3 × 5 min in TBS-T. Anti-mouse IgG, horseradish peroxidase conjugated (1:1000, ECL), was applied to sections and incubated 45 min, then washed 3 × 5 min in TBS-T. DAB chromogen reagent (Vector Laboratories, Burlington, ON, Canada) was applied, and sections were rinsed with distilled water when the desired level of target to background staining was achieved. Sections were counterstained with Mayer's hematoxylin and dehydrated, and coverslips were applied. Slides were examined under a light microscope (Zeiss Axiovert 200M, Carl Zeiss Canada, Toronto, ON, Canada), and representative images were captured at 50×, 200×, and 400× magnification using a Leica DC300 digital camera and software (Leica Microsystems Canada Inc., Richmond Hill, ON).

Anti-AβO^{cSNK} Injection Mouse Studies. Twenty-four retired male Tg2576 breeders were purchased from Taconic. Twenty-four APP/PS1 heterozygote animals of each sex, coexpressing a chimeric mouse/human APP650 cDNA containing the Swedish (KM670/671NL) mutations and the human presenilin 1 (PS1) gene containing the ΔE9 mutation,[81] were bred on a F1:C3H/C57Bl/6 background and aged in house. At 12 months of age, Tg2576 and APP/PS1 mice were treated weekly by ip injection (500 μg initial dose followed by weekly 1000 μg) with anti-AβO^{cSNK} or nonspecific murine IgG1 control (provided by Cangene Corp, now Emergent BioSolutions) for 6 weeks. At sacrifice, animals were perfused prior to harvesting of brains. One hemibrain from each animal was fixed in 4% PFA, while the other hemibrains were stored frozen.

Soluble aggregated Aβ was assayed in soluble brain extracts using the Amorfix Aggregated Aβ A^4 Assay (Amorfix Life Sciences, Toronto, ON,

DOI: 10.1021/acschemneuro.7b00469
ACS Chem. Neurosci. 2018, 9, 1591−1606

Canada, now ProMIS Neurosciences). Hemibrains were homogenized in RIPA buffer followed by serial centrifugation including 100 000*g* for 1 h to generate a brain homogenate containing only soluble proteins (i.e., soluble AβOs). The soluble brain extracts were then analyzed by Amorfix in comparison to an $A\beta_{40}$ standard curve.

Distributional analysis was performed using Shapiro−Wilk test. Based on the distributions, variations between treatment groups were analyzed using two-tailed *t* test or two-tailed Wilcoxon−Mann−Whitney test.

$A\beta_{1-42}$ Oligomer Intracerebroventricular Injection and Novel Object Recognition. Experiments were conducted essentially as described.[4] Briefly, 7−8 weeks old male C57BL/6 mice (Charles River, Italy) were implanted with a stainless steel cannula by stereotaxic surgery (L ±1.0; DV −3.0 from dura). $A\beta O_{42}$ were infused into the lateral cerebral ventricle using an injection unit inserted into the guide cannula. AβO were diluted to 1 μM in 5 mM PBS, pH 7.4,[4] in the presence or absence of either anti-$A\beta O^{cSNK}$ or mouse IgG1 at 1 μg/25 μL for 1 h on ice. Portions (7.5 μL) of these mixtures were infused into the animals using a Hamilton syringe in a total time of 5 min. The injection unit was left in place for 2 min more to allow the liquid to diffuse. Recognition memory was measured using an open-square gray arena and various objects of different sizes and materials. The task started with a habituation trial on day 1 followed by a familiarization trial (day 2) in which two identical objects were presented to the animals, and the test trial (day 3) where one familiar object was substituted with a novel one, as detailed.[4]

Active Immunization with cSNK-KLH. Sex matched cohorts of 38 APP/PS1 mice on a C3H/C57Bl/6 background were vaccinated subcutaneously with 100 μg of cSNK-KLH every 4 weeks beginning at 3 months of age, with Emulsigen-D as an adjuvant. Control animals were injected with Emulsigen-D alone. Animals received 11 treatments, and plasma was collected once prior to treatment and at monthly intervals thereafter. At 11 months of age, the animals were tested in the cued and contextual FC tasks. Following sacrifice at 12 months of age, plaque load was determined with ThioS staining, and aggregated Aβ was measured by the A^4 assay (performed by QPS Austria, Grambach).

Titer Assay. Antibodies to cSNK and to $A\beta O_{42}$ were detected using a Molecular Affinity Screening System (MASS-1; Sierra Sensors, Germany), a high throughput surface plasmon resonance imaging analytical biosensor. cSNK-BSA and BSA were immobilized on separate flow cells of a sensor chip, and serial plasma samples of all 76 mice were injected over the surface. Likewise, in a separate set of experiments, synthetic $A\beta_{42}$ oligomers were immobilized, and serial plasma samples of 12 randomly selected mice with antibodies to cSNK were analyzed. Early stage stable binding is reported for both assays.

Immunoglobulin Isotype and IgG Subclass. Serial plasma samples of 12 randomly selected mice with antibodies to cSNK were analyzed. Using HBS-EP-BSA (10 mM HEPES pH 7.4, 150 mM NaCl, 3 mM EDTA, 0.005% v/v with 0.2% w/v BSA) as sample and running buffer, we diluted plasma samples 1/100 and injected them into the MASS1 over $A\beta O_{42}$ and BSA reference surfaces for 3 min at a flow rate of 5 μL/min. Following a 3 min wash during which running buffer was flowed over the surfaces, purified goat anti-mouse IgA, IgM, IgG, IgG1, IgG2a, IgG2ab, IgG2c, and IgG3 (Biolegend) at concentrations of 50 μg/mL, were sequentially injected over the bound antibodies for 2 min, followed by a 1 min dissociation phase. At the end of each cycle, the sensor chip surface was regenerated with 1 min injection of Glycine-HCl, pH 1.5. Resultant sensorgrams were double-referenced by subtracting blank injections, and BSA reference surface binding and binding response report points were collected. For each immunized mouse, baseline binding response was subtracted from all subsequent time points.

Contextual and Cued Fear Conditioning Tasks. Contextual and cued FC tasks were utilized to assess learning and memory as described in accordance to previously detailed methods.[82]

Training. During training, mice were placed in an illuminated compartment of a shuttle box (Med Associates Inc.) and allowed to habituate to the internal testing environment for 120 s. After the habituation period, an 80 dB auditory cue was played for 30 s. During the last 2 s of the auditory cue, a mild foot shock (0.8 mA) was administered. After shock presentation, mice were left undisturbed in the testing chamber for an intertrial interval (ITI) of 60 s. After the ITI mice were presented with a second identical tone, shock trial.

Context Testing. Twenty-four hours after training, mice were tested for their ability to remember the context in which they received the foot shock. Mice were placed in the same illuminated compartment and observed for the presence/absence of a freezing response over 5 min. During this time, mice were not exposed to the tone or shock.

Cued Testing. Four hours post-context-testing, mice were tested for their ability to remember the 80 dB auditory cue presented during the training session. Testing was conducted in an environment different from the training and context testing session (darkened compartment, false floor placed over the steel rods of the shuttle box, different cleaning solution). Mice were placed in the darkened compartment and allowed to habituate for 120 s, followed by the 80 dB auditory cue for 120 s. After the tone presentation, mice were left undisturbed in the testing chamber for 60 s.

Statistical Analysis. The Shapiro−Wilk test was performed throughout to test data normality. Differences between groups and sexes were tested using a regression model with categorical covariates (ANOVA) or *t* test or Mann−Whitney test when appropriate; we used XLSTAT V2014.6.04 and GraphPad Prism for statistical analysis. Standard error measurement (SEM) was determined throughout.

■ ASSOCIATED CONTENT

Supporting Information

The Supporting Information is available free of charge on the ACS Publications website at DOI: 10.1021/acschemneuro.7b00469.

Supporting methods for atomic force microscopy of Aβ species, binding of anti-$A\beta O^{cSNK}$ to scrambled Aβ oligomers, immunohistochemistry of mouse brain sections, and immunoblotting of Aβ aggregation assay and additional computational analysis, confirmation of epitope specificity, and aggregation related data (PDF)

■ AUTHOR INFORMATION

Corresponding Author

*Neil R. Cashman. E-mail: neil.cashman@vch.ca. Phone: 604 822-2135.

ORCID

Judith M. Silverman: 0000-0001-8299-7155

Author Contributions

[▽]J.M.S. and E.G. contributed equally to the work. N.R.C. conceptualized the cSNK epitope and generated the anti-$A\beta O^{cSNK}$ antibody. J.M.S., E.G., C.L.W., and N.R.C. designed and interpreted the experiments. X.P. and S.S.P. performed computational studies of cSNK. K.M.M., J.W., G.L., S.L., Y.B., C.M.C., J.R., S.S., C.B., and G.-Y.R.H. also participated in experimental design and conducted experiments. J.M.S., C.L.W., S.S.P., and N.R.C. prepared the manuscript.

Funding

We thank the Canadian Institutes of Health Research, PrioNet Canada, Brain Canada, the Alberta Innovates Bio Solutions, the Canadian Consortium on Neurodegeneration in Aging, Cangene Corporation and Emergent BioSolutions, and the Giancarlo and Odette Tognetti Trust Foundation for the funding to undertake these studies. The Paul Heller Memorial Fund overseen by the Vancouver Foundation, PrioNet Canada, and Cangene Corporation provided stipend support for J.M.S.

Notes

The authors declare the following competing financial interest(s): ProMIS Neurosciences has an option to develop the cSNK technology, owned by the University of British

DOI: 10.1021/acschemneuro.7b00469
ACS Chem. Neurosci. 2018, 9, 1591−1606

Columbia. Dr. Cashman and Dr. Plotkin are Chief Scientific and Physics Officers, respectively, of ProMIS Neurosciences.

■ ACKNOWLEDGMENTS

The authors thank John-Paul Heale (Director UBC UILO) and Laura Saward (Emergent Biosolutions) for their guidance and championship of the project, Weihong Song for materials, Luke McAlary, Hongbin Li, Joerg Gsponer, Nicolay Blinov, and Andriy Kovalenko for contributing discussions, and Cory Nykiforuk and Xiaobing Han with Emergent BioSolutions for their contributions to data collection.

■ ABBREVIATIONS

AβO, oligomers of amyloid-β; AD, Alzheimer's disease; cSNK, cyclic-serine−asparagine−lysine; AβO^{cSNK}, amyloid-β oligomers displaying the cSNK epitope; SPR, surface plasmon resonance; CSF, cerebral spinal fluid; ARIA-E, amyloid-related imaging abnormalities−edema

■ REFERENCES

(1) Walsh, D. M., Klyubin, I., Fadeeva, J. V., Cullen, W. K., Anwyl, R., Wolfe, M. S., Rowan, M. J., and Selkoe, D. J. (2002) Naturally secreted oligomers of amyloid beta protein potently inhibit hippocampal long-term potentiation in vivo. *Nature 416*, 535−539.

(2) Cleary, J. P., Walsh, D. M., Hofmeister, J. J., Shankar, G. M., Kuskowski, M. A., Selkoe, D. J., and Ashe, K. H. (2005) Natural oligomers of the amyloid-beta protein specifically disrupt cognitive function. *Nat. Neurosci. 8*, 79−84.

(3) Lauren, J., Gimbel, D. A., Nygaard, H. B., Gilbert, J. W., and Strittmatter, S. M. (2009) Cellular prion protein mediates impairment of synaptic plasticity by amyloid-beta oligomers. *Nature 457*, 1128−1132.

(4) Balducci, C., Beeg, M., Stravalaci, M., Bastone, A., Sclip, A., Biasini, E., Tapella, L., Colombo, L., Manzoni, C., Borsello, T., Chiesa, R., Gobbi, M., Salmona, M., and Forloni, G. (2010) Synthetic amyloid-beta oligomers impair long-term memory independently of cellular prion protein. *Proc. Natl. Acad. Sci. U. S. A. 107*, 2295−2300.

(5) Jin, M., Shepardson, N., Yang, T., Chen, G., Walsh, D., and Selkoe, D. J. (2011) Soluble amyloid beta-protein dimers isolated from Alzheimer cortex directly induce Tau hyperphosphorylation and neuritic degeneration. *Proc. Natl. Acad. Sci. U. S. A. 108*, 5819−5824.

(6) Shankar, G. M., Li, S., Mehta, T. H., Garcia-Munoz, A., Shepardson, N. E., Smith, I., Brett, F. M., Farrell, M. A., Rowan, M. J., Lemere, C. A., Regan, C. M., Walsh, D. M., Sabatini, B. L., and Selkoe, D. J. (2008) Amyloid-beta protein dimers isolated directly from Alzheimer's brains impair synaptic plasticity and memory. *Nat. Med. 14*, 837−842.

(7) Reed, M. N., Hofmeister, J. J., Jungbauer, L., Welzel, A. T., Yu, C., Sherman, M. A., Lesne, S., Ladu, M. J., Walsh, D. M., Ashe, K. H., and Cleary, J. P. (2011) Cognitive effects of cell-derived and synthetically derived Abeta oligomers. *Neurobiol. Aging 32*, 1784.

(8) De Felice, F. G., Wu, D., Lambert, M. P., Fernandez, S. J., Velasco, P. T., Lacor, P. N., Bigio, E. H., Jerecic, J., Acton, P. J., Shughrue, P. J., Chen-Dodson, E., Kinney, G. G., and Klein, W. L. (2008) Alzheimer's disease-type neuronal tau hyperphosphorylation induced by A beta oligomers. *Neurobiol. Aging 29*, 1334−1347.

(9) Panza, F., Logroscino, G., Imbimbo, B. P., and Solfrizzi, V. (2014) Is there still any hope for amyloid-based immunotherapy for Alzheimer's disease? *Curr. Opin. Psych. 27*, 128−137.

(10) Schenk, D., Hagen, M., and Seubert, P. (2004) Current progress in beta-amyloid immunotherapy. *Curr. Opin. Immunol. 16*, 599−606.

(11) Liu, Y. H., Giunta, B., Zhou, H. D., Tan, J., and Wang, Y. J. (2012) Immunotherapy for Alzheimer disease: the challenge of adverse effects. *Nat. Rev. Neurol. 8*, 465−469.

(12) Sperling, R., Salloway, S., Brooks, D. J., Tampieri, D., Barakos, J., Fox, N. C., Raskind, M., Sabbagh, M., Honig, L. S., Porsteinsson, A. P., Lieberburg, I., Arrighi, H. M., Morris, K. A., Lu, Y., Liu, E., Gregg, K. M., Brashear, H. R., Kinney, G. G., Black, R., and Grundman, M. (2012) Amyloid-related imaging abnormalities in patients with Alzheimer's disease treated with bapineuzumab: a retrospective analysis. *Lancet Neurol. 11*, 241−249.

(13) Lee, E. B., Leng, L. Z., Zhang, B., Kwong, L., Trojanowski, J. Q., Abel, T., and Lee, V. M. (2006) Targeting amyloid-beta peptide (Abeta) oligomers by passive immunization with a conformation-selective monoclonal antibody improves learning and memory in Abeta precursor protein (APP) transgenic mice. *J. Biol. Chem. 281*, 4292−4299.

(14) Zhang, Y., He, J. S., Wang, X., Wang, J., Bao, F. X., Pang, S. Y., Yin, F., Hu, H. G., Peng, X. L., Sun, W. M., Zheng, Y. P., Hou, L. L., and Hong, T. (2011) Administration of amyloid-β42 oligomer-specific monoclonal antibody improved memory performance in SAMP8 mice. *J. Alzheimers Dis. 23*, 551−561.

(15) Wang, X. P., Zhang, J. H., Wang, Y. J., Feng, Y., Zhang, X., Sun, X. X., Li, J. L., Du, X. T., Lambert, M. P., Yang, S. G., Zhao, M., Klein, W. L., and Liu, R. T. (2009) Conformation-dependent single-chain variable fragment antibodies specifically recognize beta-amyloid oligomers. *FEBS Lett. 583*, 579−584.

(16) Hillen, H., Barghorn, S., Striebinger, A., Labkovsky, B., Muller, R., Nimmrich, V., Nolte, M. W., Perez-Cruz, C., van der Auwera, I., van Leuven, F., van Gaalen, M., Bespalov, A. Y., Schoemaker, H., Sullivan, J. P., and Ebert, U. (2010) Generation and therapeutic efficacy of highly oligomer-specific beta-amyloid antibodies. *J. Neurosci. 30*, 10369−10379.

(17) Kayed, R., Head, E., Thompson, J. L., McIntire, T. M., Milton, S. C., Cotman, C. W., and Glabe, C. G. (2003) Common Structure of Soluble Amyloid Oligomers Implies Common Mechanism of Pathogenesis. *Science 300*, 486−489.

(18) Kayed, R., Head, E., Sarsoza, F., Saing, T., Cotman, C. W., Necula, M., Margol, L., Wu, J., Breydo, L., Thompson, J. L., Rasool, S., Gurlo, T., Butler, P., and Glabe, C. G. (2007) Fibril specific, conformation dependent antibodies recognize a generic epitope common to amyloid fibrils and fibrillar oligomers that is absent in prefibrillar oligomers. *Mol. Neurodegener. 2*, 18.

(19) Kayed, R., Canto, I., Breydo, L., Rasool, S., Lukacsovich, T., Wu, J., Albay, R., 3rd, Pensalfini, A., Yeung, S., Head, E., Marsh, J. L., and Glabe, C. (2010) Conformation dependent monoclonal antibodies distinguish different replicating strains or conformers of prefibrillar Abeta oligomers. *Mol. Neurodegener. 5*, 57.

(20) Morgado, I., Wieligmann, K., Bereza, M., Rönicke, R., Meinhardt, K., Annamalai, K., Baumann, M., Wacker, J., Hortschansky, P., Malešević, M., Parthier, C., Mawrin, C., Schiene-Fischer, C., Reymann, K. G., Stubbs, M. T., Balbach, J., Görlach, M., Horn, U., and Fändrich, M. (2012) Molecular basis of β-amyloid oligomer recognition with a conformational antibody fragment. *Proc. Natl. Acad. Sci. U. S. A. 109*, 12503−12508.

(21) Zhao, M., Wang, S. W., Wang, Y. J., Zhang, R., Li, Y. N., Su, Y. J., Zhou, W. W., Yu, X. L., and Liu, R. T. (2014) Pan-amyloid oligomer specific scFv antibody attenuates memory deficits and brain amyloid burden in mice with Alzheimer's disease. *Curr. Alzheimer Res. 11*, 69−78.

(22) Tucker, S., Moller, C., Tegerstedt, K., Lord, A., Laudon, H., Sjodahl, J., Soderberg, L., Spens, E., Sahlin, C., Waara, E. R., Satlin, A., Gellerfors, P., Osswald, G., and Lannfelt, L. (2015) The murine version of BAN2401 (mAb158) selectively reduces amyloid-beta protofibrils in brain and cerebrospinal fluid of tg-ArcSwe mice. *J. Alzheimers Dis. 43*, 575−588.

(23) Perchiacca, J. M., Ladiwala, A. R. A., Bhattacharya, M., and Tessier, P. M. (2012) Structure-based design of conformation- and sequence-specific antibodies against amyloid β. *Proc. Natl. Acad. Sci. U. S. A. 109*, 84−89.

(24) Lambert, M. P., Velasco, P. T., Chang, L., Viola, K. L., Fernandez, S., Lacor, P. N., Khuon, D., Gong, Y., Bigio, E. H., Shaw, P., De Felice, F. G., Krafft, G. A., and Klein, W. L. (2007) Monoclonal antibodies that target pathological assemblies of Abeta. *J. Neurochem. 100*, 23−35.

(25) Sevigny, J., Chiao, P., Bussiere, T., Weinreb, P. H., Williams, L., Maier, M., Dunstan, R., Salloway, S., Chen, T., Ling, Y., O'Gorman, J., Qian, F., Arastu, M., Li, M., Chollate, S., Brennan, M. S., Quintero-Monzon, O., Scannevin, R. H., Arnold, H. M., Engber, T., Rhodes, K., Ferrero, J., Hang, Y., Mikulskis, A., Grimm, J., Hock, C., Nitsch, R. M.,

DOI: 10.1021/acschemneuro.7b00469
ACS Chem. Neurosci. 2018, 9, 1591−1606

and Sandrock, A. (2016) The antibody aducanumab reduces Abeta plaques in Alzheimer's disease. *Nature 537*, 50−56.
(26) Baumketner, A., Bernstein, S. L., Wyttenbach, T., Bitan, G., Teplow, D. B., Bowers, M. T., and Shea, J. E. (2006) Amyloid beta-protein monomer structure: a computational and experimental study. *Protein Sci. 15*, 420−428.
(27) Ahmed, M., Davis, J., Aucoin, D., Sato, T., Ahuja, S., Aimoto, S., Elliott, J. I., Van Nostrand, W. E., and Smith, S. O. (2010) Structural conversion of neurotoxic amyloid-beta(1−42) oligomers to fibrils. *Nat. Struct. Mol. Biol. 17*, 561−567.
(28) Petkova, A. T., and Tycko, R. (2002) Sensitivity enhancement in structural measurements by solid state NMR through pulsed spin locking. *J. Magn. Reson. 155*, 293−299.
(29) Colletier, J. P., Laganowsky, A., Landau, M., Zhao, M., Soriaga, A. B., Goldschmidt, L., Flot, D., Cascio, D., Sawaya, M. R., and Eisenberg, D. (2011) Molecular basis for amyloid-beta polymorphism. *Proc. Natl. Acad. Sci. U. S. A. 108*, 16938−16943.
(30) Luhrs, T., Ritter, C., Adrian, M., Riek-Loher, D., Bohrmann, B., Dobeli, H., Schubert, D., and Riek, R. (2005) 3D structure of Alzheimer's amyloid-beta(1−42) fibrils. *Proc. Natl. Acad. Sci. U. S. A. 102*, 17342−17347.
(31) Sawaya, M. R., Sambashivan, S., Nelson, R., Ivanova, M. I., Sievers, S. A., Apostol, M. I., Thompson, M. J., Balbirnie, M., Wiltzius, J. J., McFarlane, H. T., Madsen, A. O., Riekel, C., and Eisenberg, D. (2007) Atomic structures of amyloid cross-beta spines reveal varied steric zippers. *Nature 447*, 453−457.
(32) Petkova, A. T., Ishii, Y., Balbach, J. J., Antzutkin, O. N., Leapman, R. D., Delaglio, F., and Tycko, R. (2002) A structural model for Alzheimer's beta -amyloid fibrils based on experimental constraints from solid state NMR. *Proc. Natl. Acad. Sci. U. S. A. 99*, 16742−16747.
(33) Lazo, N. D., Grant, M. A., Condron, M. C., Rigby, A. C., and Teplow, D. B. (2005) On the nucleation of amyloid beta-protein monomer folding. *Protein Sci. 14*, 1581−1596.
(34) Walti, M. A., Ravotti, F., Arai, H., Glabe, C. G., Wall, J. S., Bockmann, A., Guntert, P., Meier, B. H., and Riek, R. (2016) Atomic-resolution structure of a disease-relevant Abeta(1−42) amyloid fibril. *Proc. Natl. Acad. Sci. U. S. A. 113*, E4976−4984.
(35) Xiao, Y., Ma, B., McElheny, D., Parthasarathy, S., Long, F., Hoshi, M., Nussinov, R., and Ishii, Y. (2015) Abeta(1−42) fibril structure illuminates self-recognition and replication of amyloid in Alzheimer's disease. *Nat. Struct. Mol. Biol. 22*, 499−505.
(36) Gremer, L., Scholzel, D., Schenk, C., Reinartz, E., Labahn, J., Ravelli, R. B. G., Tusche, M., Lopez-Iglesias, C., Hoyer, W., Heise, H., Willbold, D., and Schroder, G. F. (2017) Fibril structure of amyloid-beta(1−42) by cryo-electron microscopy. *Science 358*, 116−119.
(37) Lambert, M. P., Barlow, A. K., Chromy, B. A., Edwards, C., Freed, R., Liosatos, M., Morgan, T. E., Rozovsky, I., Trommer, B., Viola, K. L., Wals, P., Zhang, C., Finch, C. E., Krafft, G. A., and Klein, W. L. (1998) Diffusible, nonfibrillar ligands derived from Abeta1−42 are potent central nervous system neurotoxins. *Proc. Natl. Acad. Sci. U. S. A. 95*, 6448−6453.
(38) Stroud, J. C., Liu, C., Teng, P. K., and Eisenberg, D. (2012) Toxic fibrillar oligomers of amyloid-beta have cross-beta structure. *Proc. Natl. Acad. Sci. U. S. A. 109*, 7717−7722.
(39) Kotler, S. A., Brender, J. R., Vivekanandan, S., Suzuki, Y., Yamamoto, K., Monette, M., Krishnamoorthy, J., Walsh, P., Cauble, M., Holl, M. M., Marsh, E. N., and Ramamoorthy, A. (2015) High-resolution NMR characterization of low abundance oligomers of amyloid-beta without purification. *Sci. Rep. 5*, 11811.
(40) Sinha, S., Lopes, D. H., and Bitan, G. (2012) A key role for lysine residues in amyloid beta-protein folding, assembly, and toxicity. *ACS Chem. Neurosci. 3*, 473−481.
(41) Kocis, P., Tolar, M., Yu, J., Sinko, W., Ray, S., Blennow, K., Fillit, H., and Hey, J. A. (2017) Elucidating the Aβ42 Anti-Aggregation Mechanism of Action of Tramiprosate in Alzheimer's Disease: Integrating Molecular Analytical Methods, Pharmacokinetic and Clinical Data. *CNS Drugs 31*, 495−509.
(42) Di Scala, C., Yahi, N., Boutemeur, S., Flores, A., Rodriguez, L., Chahinian, H., and Fantini, J. (2016) Common molecular mechanism of amyloid pore formation by Alzheimer's beta-amyloid peptide and alpha-synuclein. *Sci. Rep. 6*, 28781.
(43) Lu, J. X., Qiang, W., Yau, W. M., Schwieters, C. D., Meredith, S. C., and Tycko, R. (2013) Molecular structure of beta-amyloid fibrils in Alzheimer's disease brain tissue. *Cell 154*, 1257−1268.
(44) Connolly, M. L. (1983) Analytical Molecular-Surface Calculation. *J. Appl. Crystallogr. 16*, 548−558.
(45) Richmond, T. J. (1984) Solvent Accessible Surface-Area and Excluded Volume in Proteins - Analytical Equations for Overlapping Spheres and Implications for the Hydrophobic Effect. *J. Mol. Biol. 178*, 63−89.
(46) Liu, P., Reed, M. N., Kotilinek, L. A., Grant, M. K., Forster, C. L., Qiang, W., Shapiro, S. L., Reichl, J. H., Chiang, A. C., Jankowsky, J. L., Wilmot, C. M., Cleary, J. P., Zahs, K. R., and Ashe, K. H. (2015) Quaternary Structure Defines a Large Class of Amyloid-beta Oligomers Neutralized by Sequestration. *Cell Rep. 11*, 1760−1771.
(47) Caetano, F. A., Beraldo, F. H., Hajj, G. N., Guimaraes, A. L., Jurgensen, S., Wasilewska-Sampaio, A. P., Hirata, P. H., Souza, I., Machado, C. F., Wong, D. Y., De Felice, F. G., Ferreira, S. T., Prado, V. F., Rylett, R. J., Martins, V. R., and Prado, M. A. (2011) Amyloid-beta oligomers increase the localization of prion protein at the cell surface. *J. Neurochem. 117*, 538−553.
(48) Rangachari, V., Moore, B. D., Reed, D. K., Sonoda, L. K., Bridges, A. W., Conboy, E., Hartigan, D., and Rosenberry, T. L. (2007) Amyloid-beta(1−42) rapidly forms protofibrils and oligomers by distinct pathways in low concentrations of sodium dodecylsulfate. *Biochemistry 46*, 12451−12462.
(49) Mastrangelo, I. A., Ahmed, M., Sato, T., Liu, W., Wang, C., Hough, P., and Smith, S. O. (2006) High-resolution atomic force microscopy of soluble Abeta42 oligomers. *J. Mol. Biol. 358*, 106−119.
(50) Airoldi, C., Colombo, L., Manzoni, C., Sironi, E., Natalello, A., Doglia, S. M., Forloni, G., Tagliavini, F., Del Favero, E., Cantu, L., Nicotra, F., and Salmona, M. (2011) Tetracycline prevents Abeta oligomer toxicity through an atypical supramolecular interaction. *Org. Biomol. Chem. 9*, 463−472.
(51) Yoshiike, Y., Minai, R., Matsuo, Y., Chen, Y.-R., Kimura, T., and Takashima, A. (2008) Amyloid Oligomer Conformation in a Group of Natively Folded Proteins. *PLoS One 3*, e3235.
(52) Cox, D., Selig, E., Griffin, M. D., Carver, J. A., and Ecroyd, H. (2016) Small Heat-shock Proteins Prevent alpha-Synuclein Aggregation via Transient Interactions and Their Efficacy Is Affected by the Rate of Aggregation. *J. Biol. Chem. 291*, 22618−22629.
(53) Cohen, S. I., Linse, S., Luheshi, L. M., Hellstrand, E., White, D. A., Rajah, L., Otzen, D. E., Vendruscolo, M., Dobson, C. M., and Knowles, T. P. (2013) Proliferation of amyloid-beta42 aggregates occurs through a secondary nucleation mechanism. *Proc. Natl. Acad. Sci. U. S. A. 110*, 9758−9763.
(54) Arosio, P., Knowles, T. P., and Linse, S. (2015) On the lag phase in amyloid fibril formation. *Phys. Chem. Chem. Phys. 17*, 7606−7618.
(55) Blennow, K., Hampel, H., Weiner, M., and Zetterberg, H. (2010) Cerebrospinal fluid and plasma biomarkers in Alzheimer disease. *Nat. Rev. Neurol. 6*, 131−144.
(56) Roe, C. M., Fagan, A. M., Grant, E. A., Hassenstab, J., Moulder, K. L., Maue Dreyfus, D., Sutphen, C. L., Benzinger, T. L., Mintun, M. A., Holtzman, D. M., and Morris, J. C. (2013) Amyloid imaging and CSF biomarkers in predicting cognitive impairment up to 7.5 years later. *Neurology 80*, 1784−1791.
(57) Joachim, C. L., Morris, J. H., and Selkoe, D. J. (1989) Diffuse senile plaques occur commonly in the cerebellum in Alzheimer's disease. *Am. J. Pathol. 135*, 309−319.
(58) Shankar, G. M., Leissring, M. A., Adame, A., Sun, X., Spooner, E., Masliah, E., Selkoe, D. J., Lemere, C. A., and Walsh, D. M. (2009) Biochemical and immunohistochemical analysis of an Alzheimer's disease mouse model reveals the presence of multiple cerebral Abeta assembly forms throughout life. *Neurobiol. Dis. 36*, 293−302.
(59) Kostylev, M. A., Kaufman, A. C., Nygaard, H. B., Patel, P., Haas, L. T., Gunther, E. C., Vortmeyer, A., and Strittmatter, S. M. (2015) Prion-Protein-interacting Amyloid-beta Oligomers of High Molecular Weight

DOI: 10.1021/acschemneuro.7b00469
ACS Chem. Neurosci. 2018, 9, 1591−1606

Are Tightly Correlated with Memory Impairment in Multiple Alzheimer Mouse Models. *J. Biol. Chem. 290*, 17415−17438.
(60) Lesne, S. E., Sherman, M. A., Grant, M., Kuskowski, M., Schneider, J. A., Bennett, D. A., and Ashe, K. H. (2013) Brain amyloid-beta oligomers in ageing and Alzheimer's disease. *Brain 136*, 1383−1398.
(61) Lesne, S., Koh, M. T., Kotilinek, L., Kayed, R., Glabe, C. G., Yang, A., Gallagher, M., and Ashe, K. H. (2006) A specific amyloid-beta protein assembly in the brain impairs memory. *Nature 440*, 352−357.
(62) Figueiredo, C. P., Clarke, J. R., Ledo, J. H., Ribeiro, F. C., Costa, C. V., Melo, H. M., Mota-Sales, A. P., Saraiva, L. M., Klein, W. L., Sebollela, A., De Felice, F. G., and Ferreira, S. T. (2013) Memantine rescues transient cognitive impairment caused by high-molecular-weight abeta oligomers but not the persistent impairment induced by low-molecular-weight oligomers. *J. Neurosci. 33*, 9626−9634.
(63) Nussbaum, J. M., Schilling, S., Cynis, H., Silva, A., Swanson, E., Wangsanut, T., Tayler, K., Wiltgen, B., Hatami, A., Ronicke, R., Reymann, K., Hutter-Paier, B., Alexandru, A., Jagla, W., Graubner, S., Glabe, C. G., Demuth, H. U., and Bloom, G. S. (2012) Prion-like behaviour and tau-dependent cytotoxicity of pyroglutamylated amyloid-beta. *Nature 485*, 651−655.
(64) Benilova, I., Karran, E., and De Strooper, B. (2012) The toxic Abeta oligomer and Alzheimer's disease: an emperor in need of clothes. *Nat. Neurosci. 15*, 349−357.
(65) Palop, J. J., and Mucke, L. (2010) Amyloid-beta-induced neuronal dysfunction in Alzheimer's disease: from synapses toward neural networks. *Nat. Neurosci. 13*, 812−818.
(66) Manuel, D. G., Garner, R., Fines, P., Bancej, C., Flanagan, W., Tu, K., Reimer, K., Chambers, L. W., and Bernier, J. (2016) Alzheimer's and other dementias in Canada, 2011 to 2031: a microsimulation Population Health Modeling (POHEM) study of projected prevalence, health burden, health services, and caregiving use. *Popul Health Metr 14*, 37.
(67) Rae, E. A., and Brown, R. E. (2015) The problem of genotype and sex differences in life expectancy in transgenic AD mice. *Neurosci. Biobehav. Rev. 57*, 238−251.
(68) Carter, C. L., Resnick, E. M., Mallampalli, M., and Kalbarczyk, A. (2012) Sex and gender differences in Alzheimer's disease: recommendations for future research. *J. Womens Health (Larchmt) 21*, 1018−1023.
(69) Audrain, M., Fol, R., Dutar, P., Potier, B., Billard, J. M., Flament, J., Alves, S., Burlot, M. A., Dufayet-Chaffaud, G., Bemelmans, A. P., Valette, J., Hantraye, P., Deglon, N., Cartier, N., and Braudeau, J. (2016) Alzheimer's disease-like APP processing in wild-type mice identifies synaptic defects as initial steps of disease progression. *Mol. Neurodegener. 11*, 5.
(70) Kaufman, A. C., Salazar, S. V., Haas, L. T., Yang, J., Kostylev, M. A., Jeng, A. T., Robinson, S. A., Gunther, E. C., van Dyck, C. H., Nygaard, H. B., and Strittmatter, S. M. (2015) Fyn inhibition rescues established memory and synapse loss in Alzheimer mice. *Ann. Neurol. 77*, 953−971.
(71) Hong, S., Beja-Glasser, V. F., Nfonoyim, B. M., Frouin, A., Li, S., Ramakrishnan, S., Merry, K. M., Shi, Q., Rosenthal, A., Barres, B. A., Lemere, C. A., Selkoe, D. J., and Stevens, B. (2016) Complement and microglia mediate early synapse loss in Alzheimer mouse models. *Science 352*, 712.
(72) Cohen, M., Appleby, B., and Safar, J. G. (2016) Distinct prion-like strains of amyloid beta implicated in phenotypic diversity of Alzheimer's disease. *Prion 10*, 9−17.
(73) Foloppe, N., and MacKerell, A. D., Jr. (2000) All-atom empirical force field for nucleic acids: I. Parameter optimization based on small molecule and condensed phase macromolecular target data. *J. Comput. Chem. 21*, 86−104.
(74) MacKerell, A. D., Bashford, D., Bellott, M., Dunbrack, R. L., Evanseck, J. D., Field, M. J., Fischer, S., Gao, J., Guo, H., Ha, S., Joseph-McCarthy, D., Kuchnir, L., Kuczera, K., Lau, F. T., Mattos, C., Michnick, S., Ngo, T., Nguyen, D. T., Prodhom, B., Reiher, W. E., Roux, B., Schlenkrich, M., Smith, J. C., Stote, R., Straub, J., Watanabe, M., Wiorkiewicz-Kuczera, J., Yin, D., and Karplus, M. (1998) All-atom empirical potential for molecular modeling and dynamics studies of proteins. *J. Phys. Chem. B 102*, 3586−3616.
(75) Jorgensen, W. L., Chandrasekhar, J., Madura, J. D., Impey, R. W., and Klein, M. L. (1983) Comparison of Simple Potential Functions for Simulating Liquid Water. *J. Chem. Phys. 79*, 926−935.
(76) Das, A., Sin, B. K., Mohazab, A. R., and Plotkin, S. S. (2013) Unfolded protein ensembles, folding trajectories, and refolding rate prediction. *J. Chem. Phys. 139*, 121925.
(77) Piana, S., et al. (2011) How robust are protein folding simulations with respect to force field parameterization? (vol 100, pg L47, 2011). *Biophys. J. 101*, 1015−1015.
(78) Paramithiotis, E., Pinard, M., Lawton, T., LaBoissiere, S., Leathers, V. L., Zou, W. Q., Estey, L. A., Lamontagne, J., Lehto, M. T., Kondejewski, L. H., Francoeur, G. P., Papadopoulos, M., Haghighat, A., Spatz, S. J., Head, M., Will, R., Ironside, J., O'Rourke, K., Tonelli, Q., Ledebur, H. C., Chakrabartty, A., and Cashman, N. R. (2003) A prion protein epitope selective for the pathologically misfolded conformation. *Nat. Med. 9*, 893−899.
(79) Rakhit, R., Robertson, J., Vande Velde, C., Horne, P., Ruth, D. M., Griffin, J., Cleveland, D. W., Cashman, N. R., and Chakrabartty, A. (2007) An immunological epitope selective for pathological monomer-misfolded SOD1 in ALS. *Nat. Med. 13*, 754−759.
(80) McKhann, G., Drachman, D., Folstein, M., Katzman, R., Price, D., and Stadlan, E. M. (1984) Clinical diagnosis of Alzheimer's disease: report of the NINCDS-ADRDA Work Group under the auspices of Department of Health and Human Services Task Force on Alzheimer's Disease. *Neurology 34*, 939−944.
(81) Jankowsky, J. L., Fadale, D. J., Anderson, J., Xu, G. M., Gonzales, V., Jenkins, N. A., Copeland, N. G., Lee, M. K., Younkin, L. H., Wagner, S. L., Younkin, S. G., and Borchelt, D. R. (2004) Mutant presenilins specifically elevate the levels of the 42 residue beta-amyloid peptide in vivo: evidence for augmentation of a 42-specific gamma secretase. *Hum. Mol. Genet. 13*, 159−170.
(82) Curzon, P., Rustay, N. R., and Browman, K. E. (2009) Cued and Contextual Fear Conditioning for Rodents, in *Methods of Behavior Analysis in Neuroscience* (Buccafusco, J. J., Ed.) 2nd ed., CRC Press, Boca Raton, FL.

DOI: 10.1021/acschemneuro.7b00469
ACS Chem. Neurosci. 2018, 9, 1591−1606

Supporting, Methods and Figures for "A Rational Conformational Epitope Defines a Distinct Subclass of Toxic Amyloid-Beta Oligomers"

Supporting Methods

Atomic Force Microscopy of Aβ species

Diluted Aβ42 monomer, oligomer, and fibril preparations were spotted on mica, washed and dried. In tapping mode, images were acquired using a Cypher AFM (Asylum Research, Santa Barbara, CA, USA) with silicon tips (AC160TS from Olympus; nominal spring constant of 40 N/m). To determine the height distribution of the various species, section analyses were performed using the AFM software.

Dot blotting

Stated amounts of $A\beta_{42}$ oligomers and prion protein oligomers (a gift from Dr. Ojer) were dotted directly onto 0.45μm nitrocellulose membranes (Pall). The membranes were probed pan Aβ antibody 6E10 (Covance, 1:1000), A11 anti-sera (Milipore, 1:500), and anti-$A\beta O^{cSNK}$ (10μg/ml).

Immunohistochemistry of mouse brain sections

Mice were cardiac perfused by PBS and posed fixed in 4% PFA for 24-48 h. Tissues were dehydrated in 30% sucrose for 48h, cryosectioned into 25-30 μm thick sections and mounted on Superfrost plus slides. Endogenous peroxidase activity was quenched using 0.5% hydrogen peroxide in methanol for 20 min. After washing 3 x 15 min in TBS, samples were put in a humidified chamber, and non-specific staining was blocked by incubation with serum-free protein blocking reagent (Dako Canada Inc., Mississauga, ON, Canada) for 1 h. For immunostaining, anti-$A\beta O^{cSNK}$ (1 μg/ml), 4G8 (1 μg/ml, Santa Cruz Biotechnology), and Iba1 (1 μg/ml, Wako Chemicals, Neuss Germany,) were used as primary antibodies. Sections were incubated overnight at 4 ºC, and washed 3 x 5 min in TBS-T. Anti-Mouse IgG Horseradish Peroxidase conjugated (1:1000, ECL) was applied to sections and incubated 45 min, then washed 3 x 5 min in TBS-T. DAB chromogen reagent (Vector Laboratories, Burlington ON, Canada) was applied and sections rinsed with distilled water when the desired level of target to background staining was achieved. Sections were counterstained with Mayer's haematoxylin, dehydrated, and cover slips were applied. Slides were examined under a light microscope (Zeiss Axiovert 200M, Carl Zeiss Canada, Toronto ON, Canada) and representative images captured at 50, 200 and 400X magnification using a Leica DC300 digital camera and software (Leica Microsystems Canada Inc., Richmond Hill, ON).

Immunoblotting and TEM of Aβ aggregation assay

HFIP-treated Amyloid beta (Aβ) peptides (BACHEM, catalogue #H-7442) were resuspended in 10 mM NaOH to a concentration of 500 μM, sonicated for 10

min, then diluted to 50 μM in 1 mM EDTA Tris-HCL buffer. They were then immediately added to a black walled 96-well plate with either buffer alone, 5 μM IgG1 isotype control, or 5 μM anti-AβO^{cSNK}, for a final volume of 100 μL and an antibody:Aβ molar ratio of 1:10. Assay controls included buffer alone, and antibody only, and treatment groups were tested in duplicates. Thioflavin T (10 μM final) was incubated with sample at room temperature for 6, 18, 30, 48 and 72 hours, readings taken every hour at 440 nm excitation and 485 nm emission.
For every time-point, samples were collected and the wells washed with 10 mM NaOH. The collected samples were centrifuged at 18,000g for 14 min at 4C, and pellets were resuspended in 10 mM NaOH. Supernatants and pellets were boiled and resolved on SDS-PAGE before immunoblotting with a pan-Aβ antibody (Rabbit anti-Aβ1-14, 1 ug/mL, Abcam). Duplicates of samples for measurement of ThioT by [platereader] were prepared in parallel, and frozen at each timepoint studied (6, 30, 48 and 72 hours). These samples were then thawed on ice for analysis by TEM. Samples were diluted 2:3 in filtered distilled water, and 5μl spotted on each carbon/formvar-coated Ni grid for 10 minutes; excess liquid was blotted away, and the grids allowed to air dry. Grids were stained with 1% aqueous uranyl acetate for 1 min, and air dried again. TEM was performed as described above.

Supporting Figures

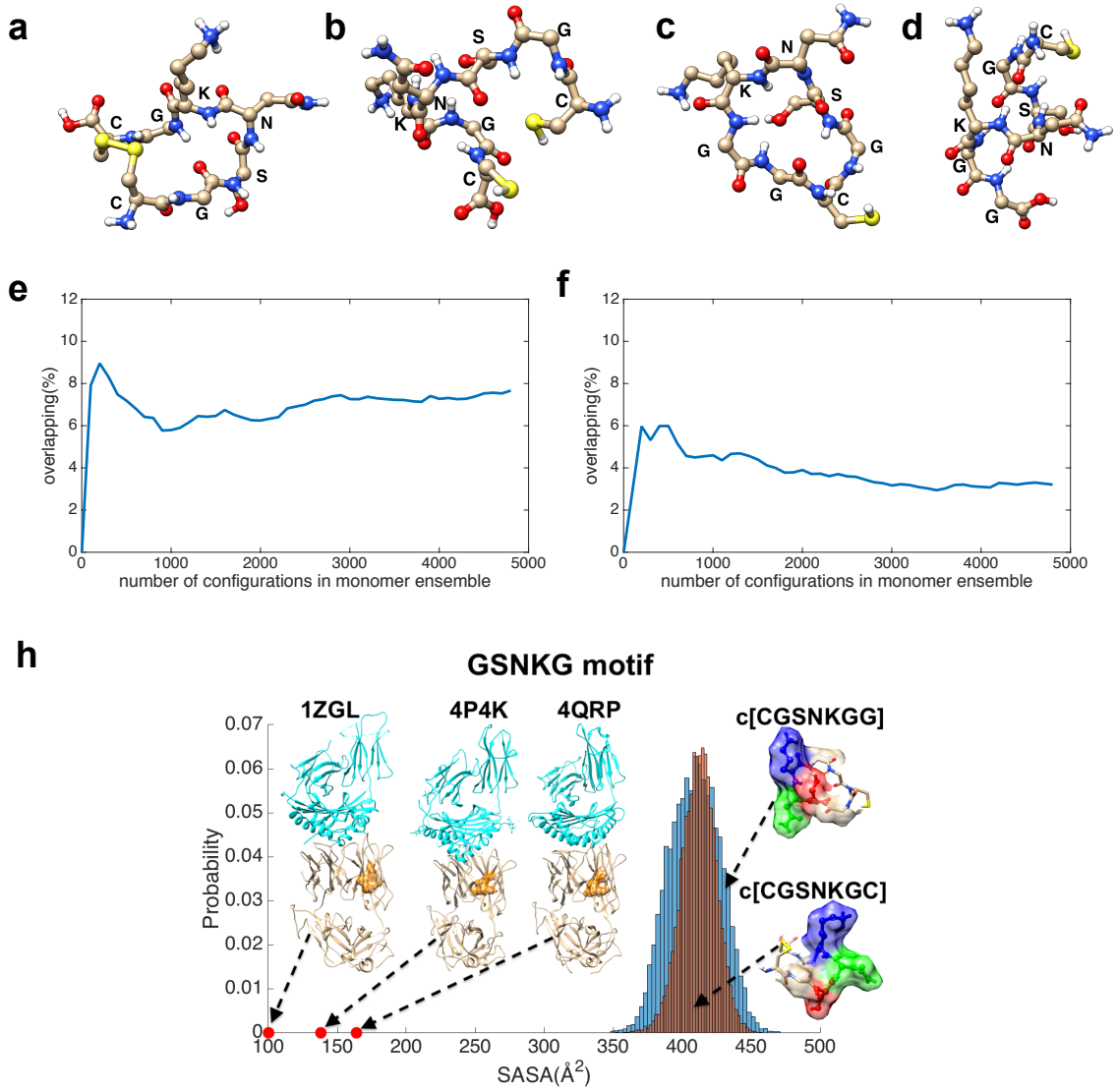

Supporting Figure 1. **cSNK has a unique structure distinct from Aβ monomers and fibrils. a-d**) Peptides synthesized for experiments. **a**) c[CGSNKGC] was cyclized via disulfide oxidation. **b**) Unstructured CGSNKGC. **c**) c[CGSNKGG] was cyclized head-to-tail with a peptide bond. **d**) Unstructured CGSNKGG. **e**,**f**) Percentage of overlap in conformation ensembles between $A\beta_{42}$ monomer and cSNK peptides c[CGSNKGC] (**e**) and c[CGSNKGG] (**f**). **h**) The solvent accessible surface area (SASA) of the GSNKG motif in three structures of the alpha chain of the variable domain of T-cell receptor protein and for the conformational ensembles of the cyclic peptide constructs c[CGSNKGG] and c[CGSNKGC]. The solvent-accessible surface of the GSNKG motif is highlighted in orange in the T-cell receptor structures (PDB: 1ZGL, 4P4K, 4QRP). Schematics of representative centroid structures for the cyclic peptides are also shown.

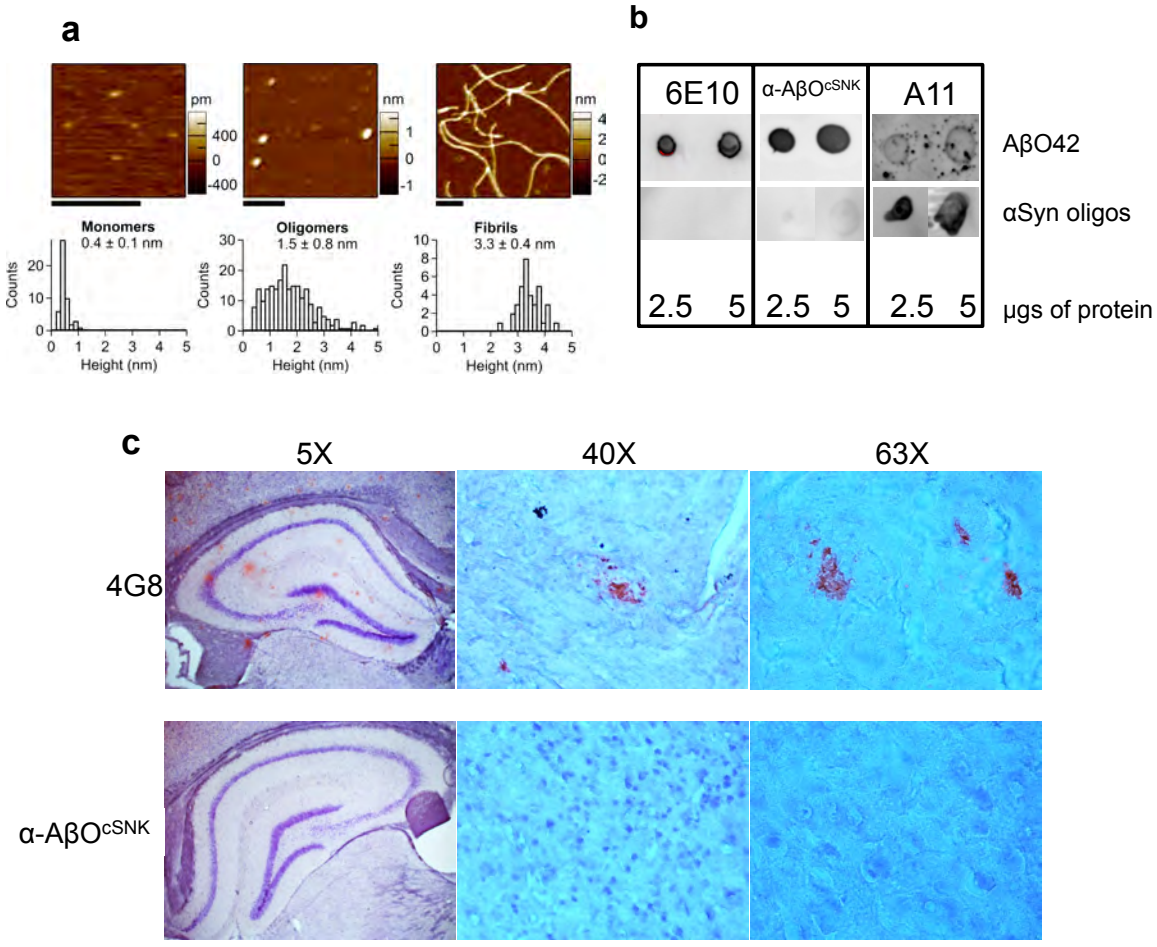

Supporting Figure 2. **Anti-AβO^{cSNK} is specific to AβO42 and does not bind Aβ plaque.** **a**) Atomic force microscopy images and height distributions of Aβ42 monomers, oligomers (AβO42), and fibrils generated at 4°C after 7 days incubation. Scale bar: 200 nm, for all images. **b**) Dot blots of AβO42 and α-synuclein oligomers (αSyn oligos) probed with 6E10, anti-AβO^{cSNK} (α-AβO^{cSNK}) and the oligomer specific antibody A11. **c**) Immunohistochemistry of the hippocampus of a male 13 month old APP/PS1 mouse. Sections were stained with 1 μg/mL 4G8 and 50 μg/mL anti-AβO^{cSNK}. Images of the hippocampus collected from the same area under increasing optical magnification. For **a-c**) data are from one of three identical experiments.

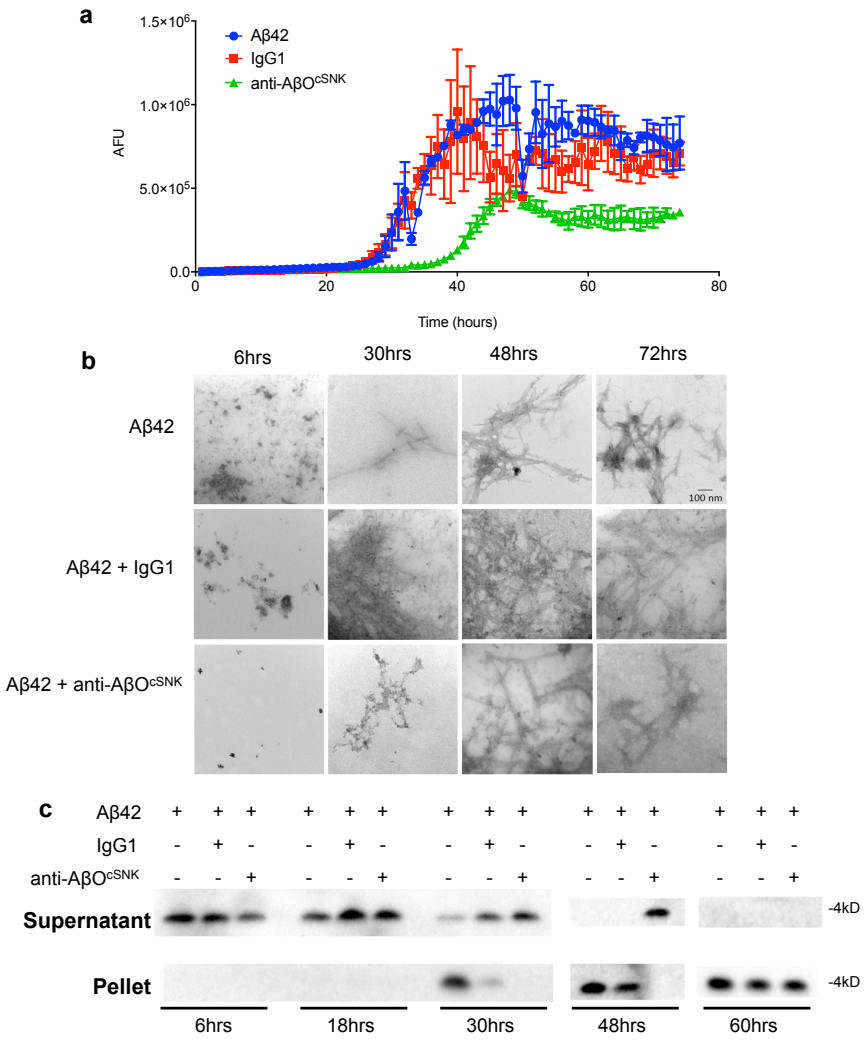

Supporting Figure 3. **Anti-AβO^{cSNK} markedly delays the aggregation of Aβ into an insoluble aggregate. a**) Beta-sheet formation was tracked for 6, 18, 30, 48 and 72 hours *in vitro* by a Thioflavin-T fluorescent assay after addition of Aβ monomers alone, or in the presence of either anti-AβO^{cSNK} or a non-specific IgG1 isotope control at a molar ratio of 10:1 Aβ:antibody. Error bars are SEM. **b**) Samples were collected at representative time points and imaged by TEM. Scale bar is applicable to all images and is 100nm. **c**) Samples were collected at representative time points and fractionated into soluble (Supernatant) or insoluble (Pellet) Aβ by centrifugation, then resolved on SDS-PAGE for immunoblotting with pan-Aβ antibody. Aβ gradually converts to its insoluble form starting at 30 h in the absence of antibody, while anti-AβO^{cSNK} retains it in its soluble form for a longer time (> 48 h). IgG1 seems to have an effect, but the delay is less pronounced than with anti-AβO^{cSNK} (between 30 and 48 h). Shown are representative data from one of three identical experiments.

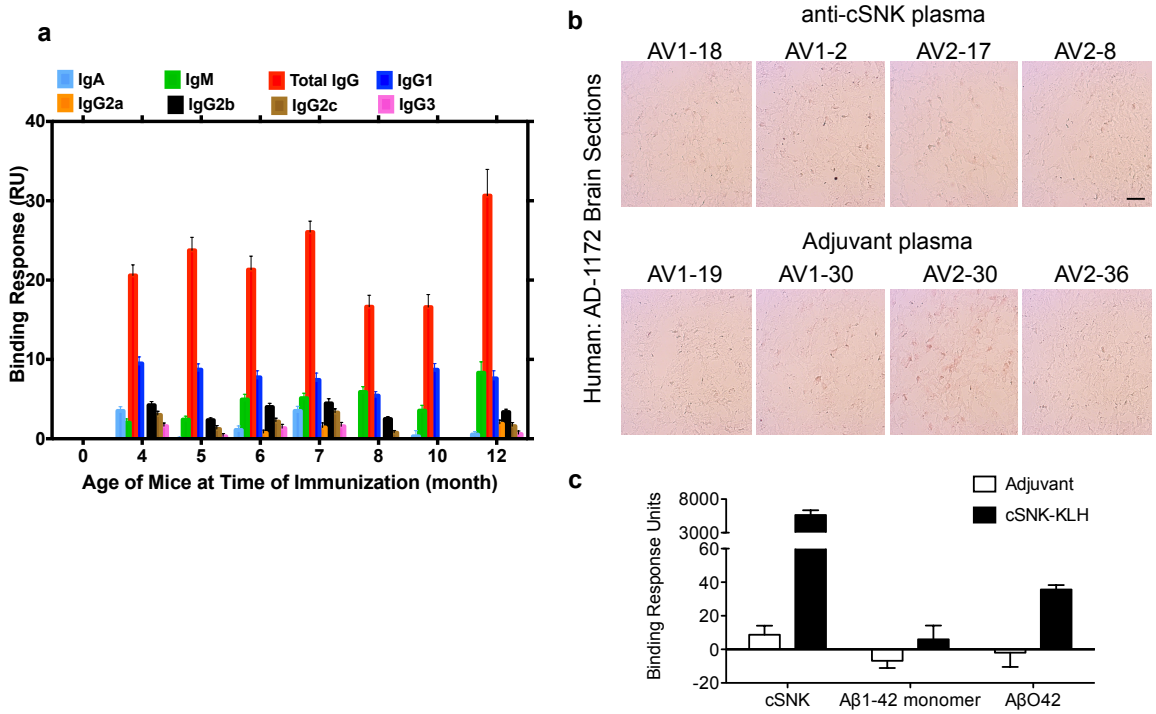

Supporting Figure 4. **No antigenic drift occurs upon repeated vaccination with cSNK. a**) Immunoglobulin isotyping of cSNK induced polyclonal response was determined by surface plasmon resonance imaging. IgG is the dominant class with IgG1 in the majority. At endpoint, IgM is approximately equal to IgG1 levels. **b**) Human AD brain sections from the frontal cortex Brodmann 9 region were probed with plasma, collected after 8 months of injections, from cSNK and adjuvant treated animals. Based on the titer data (see Fig. 5), sections were probed with approximately 1 µg/ml of anti-cSNK IgG. Since no anti-cSNK response was detected in adjuvant treated animals, we tested an equivalent volume of anti-adjuvant plasma as the anti-cSNK plasma. Scale applies to all images = 50 µm. **c**) Baseline and 8 months post-vaccination plasmas from Adjuvant and cSNK-KLH treated animals were analyzed by SPR for binding to cSNK-BSA peptide, monomeric Aβ1-42, and AβO42. Binding of the 8 month plasma to the antigens was normalized to the baseline values for each animal. SEM is shown throughout.

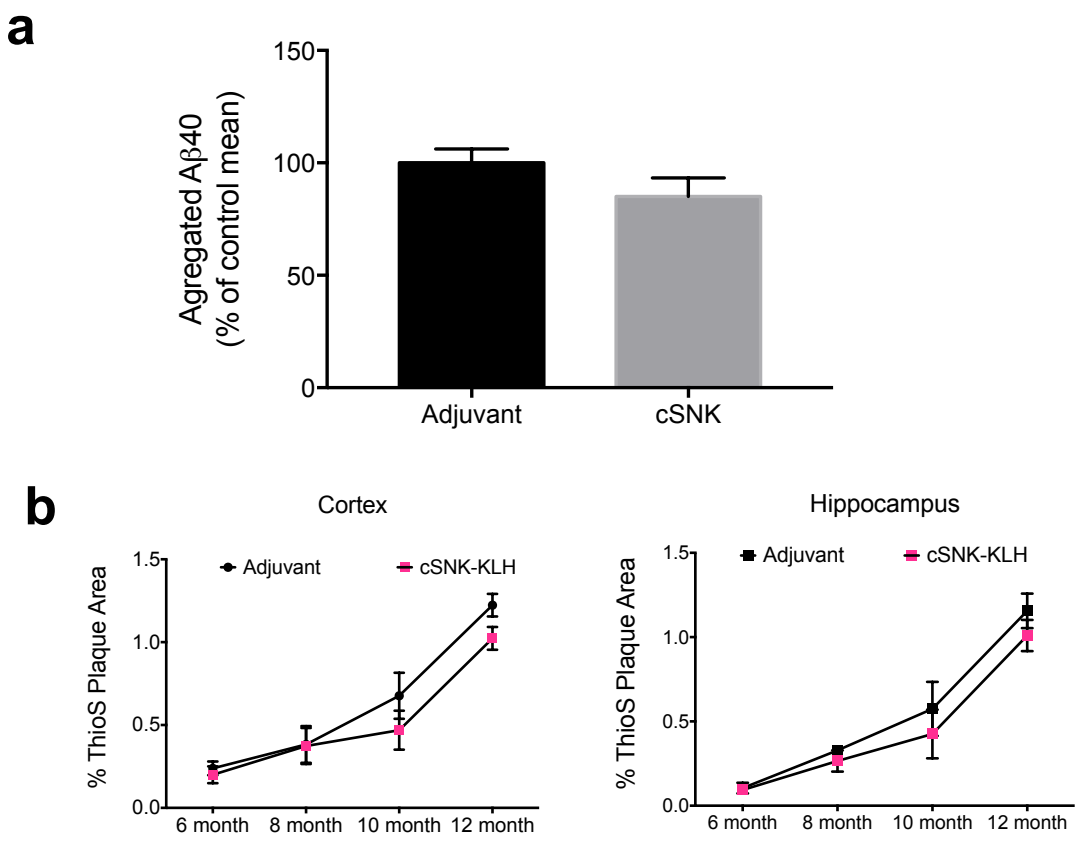

Supporting Figure 5. **Total aggregated Aβ burdens were largely unaffected by cSNK vaccination. a)** AβO levels in the brain were not affected by cSNK vaccination (p=0.0782 Mann-Whitney two-tailed, unpaired T-test; p=0.290 regression model ANOVA see Table 2). **b)** Small differences in percent of ThioS positive plaque area were found in the animals treated to endpoint (12 month) in the cortex (p=0.077), but not in the hippocampus (p=0.484). Both p values are reporting from a regression model with categorical covariates (ANOVA), see Table 2. SEM is shown throughout.